FORECASTERS' FORUM

Investigation of Cloud-to-Ground Flashes in the Non-Precipitating Stratiform Region of a Mesoscale Convective System on 20 August 2019 and Implications for Decision Support Services

CHRISTOPHER J. SCHULTZ,[a] ROGER E. ALLEN,[b] KELLEY M. MURPHY,[c] BENJAMIN S. HERZOG,[d] STEPHANIE A. WEISS,[e] AND JACQUELYN S. RINGHAUSEN[f]

[a] *NASA Short-term Prediction and Research Transition Center, Marshall Space Flight Center, Huntsville, Alabama*
[b] *NASA SPoRT/Jacobs Engineering, Huntsville, Alabama*
[c] *NASA SPoRT/Earth System Science Center, University of Alabama in Huntsville, Huntsville, Alabama*
[d] *National Weather Service, St. Louis, Missouri*
[e] *Department of Geosciences, Texas Tech University, Lubbock, Texas*
[f] *Department of Atmospheric Science, University of Alabama in Huntsville, Huntsville, Alabama*

(Manuscript received 16 June 2020, in final form 18 February 2021)

ABSTRACT: Infrequent lightning flashes occurring outside of surface precipitation pose challenges to Impact-Based Decision Support Services (IDSS) for outdoor activities. This paper examines the remote sensing observations from an event on 20 August 2019 where multiple cloud-to-ground flashes occurred over 10 km outside surface precipitation (lowest radar tilt reflectivity < 10 dBZ and no evidence of surface precipitation) in a trailing stratiform region of a mesoscale convective system. The goal is to demonstrate the fusion of radar with multiple lightning observations and a lightning risk model to demonstrate how reflectivity and differential reflectivity combined provided the best indicator for the potential of lightning where all of the other lightning safety methods failed. A total of 13 lightning flashes were observed by the Geostationary Lightning Mapper (GLM) within the trailing stratiform region between 2100 and 2300 UTC. The average size of the 13 lightning flashes was 3184 km^2, with an average total optical energy of 7734 fJ. A total of 75 NLDN flash locations were coincident with the 13 GLM flashes, resulting in an average of 5.8 NLDN flashes [in-cloud (IC) and cloud-to-ground (CG)] per GLM flash. In total, five of the GLM flashes contained at least one positive cloud-to-ground flash (+CG) flash identified by the NLDN, with peak amplitudes ranging between 66 and 136 kA. All eight CG flashes identified by the NLDN were located more than 10 km outside surface precipitation. The only indication of the potential of these infrequently large flashes was the presence of depolarization streaks in differential reflectivity (Z_{DR}) and enhanced reflectivity near the melting layer.

KEYWORDS: Lightning; Precipitation; Thunderstorms; Radars/Radar observations; Nowcasting; Operational forecasting

1. Introduction

The implementation of Geostationary Lightning Mapper (GLM) data (Goodman et al. 2013; Rudlosky et al. 2019) into the weather enterprise provides a new valuable tool to the Impact-Based Decision Support (IDSS) for operational end users. The spatial coverage of the instruments and the additional characteristics of lightning like flash area and flash energy discerned from these new measurements provide additional context to the underlying convective state of the cloud (Bruning and MacGorman 2013). Recent efforts have shown the utility of the spatial information from GLM for safety (e.g., Stano et al. 2019) and methods for fusion of these data with other satellite and radar based products to anticipate first lightning for effective lightning messaging (Elsenheimer and Gravelle 2019). Detection of early onset of electrification radar based techniques that use reflectivity at specific isotherms (e.g., Gremillion and Orville 1999; Vincent et al. 2003) and the presence of graupel within the mixed phase region of a thunderstorm (e.g., Woodard et al. 2012; Preston and Fuelberg 2015) have proven fruitful for detection of lightning potential prior to lightning occurrence. Early anticipation of flash initiation is important because as much as 20% of the time, the first flash in a storm is a cloud-to-ground (CG) flash (Schultz et al. 2017).

IDSS is direct engagement with core partners to provide important meteorological interpretation, advice, and forecasts for decisions surrounding an event, incident, or general public safety. Meteorologists performing IDSS can be at the location of the event, stakeholder operations room, or working from the NWS forecast office. Examples of IDSS where lightning data are commonly used include safety at large event venues, airport weather warnings, wildfire operations (e.g., incident meteorologists), and postevent storm recovery operations. One area of growth within lightning IDSS is identification of regions of cloud where there is potential for lightning propagation (and thus potential CG activity) because of new lightning instruments like GLM and the availability of polarimetric radar information to the operational community. A single lightning flash can propagate several hundred km and come to ground in multiple locations (e.g., Lang et al. 2017; Lyons et al. 2020; Peterson et al. 2020). Mechanisms for the generation of large flashes have been examined in the two decades to understand the development and propagation of these large powerful events (e.g., Carey et al. 2005; Steiger et al. 2007; Kuhlman et al. 2009; Weiss et al. 2012; Lyons et al. 2020). The

Corresponding author: Dr. Christopher J. Schultz, christopher.j.schultz@nasa.gov

DOI: 10.1175/WAF-D-20-0095.1

infrequency of these large flash events can create situations where lightning safety protocols (e.g., 30/30 rule, Lengyel et al. 2005) are no longer in effect when secondary flashes occur (e.g., Stano et al. 2010, 2019).

Less frequently studied are events where lightning comes to ground unexpectedly outside of surface precipitation after traveling horizontally through an anvil or trailing stratiform region (e.g., Krehbiel et al. 2008; Fuelberg et al. 2014). These events are observed by the National Lightning Detection Network (NLDN; Cummins and Murphy 2009) or Earth Networks Total Lightning Network (Liu and Heckman 2012); however, the NLDN and ENTLN[1] only provide a single latitude, longitude, peak amplitude, and in-cloud (IC) or CG designation. Thus, inferring the spatial and/or temporal evolution of the IC electrification and subsequent lightning from this data alone can prove difficult. There are a limited number of locations with two- or three-dimensional mapping of lightning (e.g., lightning mapping arrays, interferometers, low Earth orbit optical and VHF lightning observations), but their coverage and real-time availability is very limited. This is why one area of growth in nowcasting lightning is the fusion of GLM's spatial information on lightning events from operationally used ground based lightning measurements like the NLDN or ENTLN and radar measurements, to enhance IDSS.

This paper examines lightning IDSS in the context of infrequent, large, lightning flashes that occasionally came to ground more than 10 km or more outside of surface precipitation on 20 August 2019 in the National Weather Service (NWS) St. Louis's county warning area (CWA). The goal of this study is to demonstrate how the fusion of information from ground and space-based information can aid forecasters in the communication of infrequent lightning to stakeholders by using the strengths of each measurement to characterize the potential for large lightning flashes and CG activity. Objectives of the present study include:

1) Identify the flash size, flash optical energy, and polarity information of each stratiform lightning event from the 20 August 2019 case.
2) Demonstrate how two different types of lightning observations can provide unique and complementary information for decision support services to identify the flash source region and account for challenges of parallax between GLM and NLDN.
3) Understand the correspondence between GLM, the NLDN, and radar-based indicators of electrification, such as depolarization streaks and reflectivity enhancements near the melting level in ground based radar data, to anticipate the potential for ground strikes from stratiform clouds where lightning activity is infrequent.
4) Discuss this event from the perspective of current safety protocols and a lightning risk model to examine the evolution of the lightning threat at a hypothesized IDSS location. We chose the terminus of the first CG flash (38.378°N, 90.730°W) as the hypothesized IDSS location to demonstrate how radar and lightning data can be combined to aid in decision making for infrequent flashes in a stratiform region.

[1] While ENTLN is not utilized in this study, it is mentioned because it provides lightning in a similar point-based manner, and can be substituted for the NLDN if ENTLN is the only available IC and CG discriminating dataset in the forecaster's toolbox.

2. Data and methods

a. *Lightning data*

1) Geostationary lightning mapper data and imagery

GLM is a near-infrared sensor aboard the GOES-R series of satellites that measures optical brightness from lightning and other luminous events (e.g., meteorite explosions; Rumpf et al. 2019) in a 1-nm window centered on 777.4 nm (Goodman et al. 2013; Rudlosky et al. 2019). GLM consists of a charged coupled device (CCD) array that samples every 2 ms at a nadir resolution of 8 km × 8 km and ~9 km × ~14 km at the edges of the field of view. The three basic parameters of GLM are events, groups, and flashes. A GLM event is detection of photons in a CCD pixel above a background threshold in a 2-ms window. A GLM group is all contiguous GLM events that occur in the same 2-ms window. A GLM flash is an aggregation of all GLM groups that occur in the same 330-ms window and within 16.5 km of another GLM group within the same 330-ms period. The maximum duration a flash is allowed to last in the Level-2 data is 3 s or 101 contiguous groups, and these criteria were chosen to speed up real-time processing (Peterson 2019). These criteria are the standard spatial and temporal criteria used to generate the Level-2 GLM flash information disseminated from NOAA for public consumption (Rudlosky et al. 2019). GLM has an average detection efficiency of 77% over the entire field of view during a 24-h period (Bateman and Mach 2020).

Several products are derived from these base level data and utilized in this analysis: flash area (km^2), total optical energy (summation of the energy of all pixels), and flash extent density (i.e., number of lightning channels that propagate through a single 2-km advanced baseline imager pixel). All imagery are generated using the GLM tools Python library (Bruning et al. 2019). The present GLM processing algorithm used to generate the Level-2 flash algorithm artificially splices large flashes because of strict temporal maximum of 3 s and/or a maximum of 101 GLM groups to define a flash (Peterson 2019). These thresholds were implemented to speed up real-time Level-1B processing to meet the operational timing requirements of the GLM data (Mach 2019). Peterson (2019) determined that these thresholds split approximately 3% of the total flash population, specifically larger flashes. When the 3-s and 101 GLM group thresholds are relaxed, the full spatial and temporal extent of the largest flashes observed by GLM can be fully resolved by the flash clustering algorithm (Peterson 2019). These changes have not been implemented in the Level-2 data stream used in NWS operations, so both the Peterson (2019) method and the flash information from the Level-2 GLM netcdf files are presented in this study. Average flash size and energy per flash are computed using the Peterson (2019) method.

2) NATIONAL LIGHTNING DETECTION NETWORK DATA

The NLDN has been used operationally for lightning safety applications for several decades (e.g., Cummins and Murphy 2009; Holle et al. 2016). The NLDN operates in the low frequency range between 1 and 350 kHz and consists of 113 sensors across the United States (Buck et al. 2014). The NLDN has a reported detection efficiency of CG flashes between 90% and 95%, with spatial errors in CG location that are typically less than 500 m (Cummins and Murphy 2009; Buck et al. 2014; Koshak and Solakiewicz 2015; Nag et al. 2015; Medici et al. 2017). As of 2019, it is estimated that the NLDN can detect 40%–50% of IC lightning (Buck et al. 2014; Nag et al. 2015; Medici et al. 2017). Both IC and CG information is utilized in this analysis to determine the locations in which the flash remained in the cloud, and where it came to ground. Multiple NLDN flashes can be assigned to a single GLM flash (e.g., Schultz et al. 2017; Harkema et al. 2019; Lyons et al. 2020) because GLM provides a metric of the flash's areal extent, while NLDN provides specific latitude and longitude locations of rapid changes in the vertical electric field (Cummins and Murphy 2009; Nag et al. 2015).

3) GLM TOOLS SOFTWARE PACKAGE

The GLM tools software package from Bruning et al. (2019) was used for this analysis in order to match the operational implementation of GLM data for the National Weather Service (NWS) Advanced Weather Interactive Processing Systems (AWIPS; NOAA 2020). Products generated for this analysis from GLM were flash extent density (FED), average flash area (AFA), and total optical energy (TOE) in 1-min sampling periods. NLDN flash data were overlaid on the GLM images for the same 1-min periods and include cloud and ground flash designation, as well as polarity information for the CG flashes.

4) INTEGRATION OF INFORMATION FROM GLM AND NLDN

Lightning data from the NLDN and GLM were combined using a multistep method similar to Harkema et al. (2019), utilizing the methods of Peterson (2019) to mitigate flash splitting. All GLM flashes where at least one GLM event was observed to occur within 40 km (25 mi) of the hypothesized IDSS location were identified using the GLM tools software package. The ten 1-min periods with multiple GLM flashes were identified between 2100 and 2300 UTC. Next, group-level information from the Level-2 GLM data were reprocessed into flashes removing the 3 s and 101 group thresholds to mitigate artificial splitting of the lightning event by GLM's Lightning Cluster Filter algorithm. These flashes were used to interrogate the flash level information from the Level-2 GLM data to determine the number of times each GLM flash was split by the processing algorithm.

NLDN data were searched using the reprocessed GLM flash data. All NLDN IC and CG flash locations that fell within a 15-km buffer of each GLM flash footprint (to address parallax) and within 1 s of the start or end time of the GLM flash (to address any time biases) were included, following Harkema et al. (2019). Additionally, NLDN flashes that occurred within 50 km of the hypothesized IDSS location the terminus of the first CG flash (38.378°N, 90.730°W) between 2140 and 2222 UTC were added to ensure missed detections by the GLM did not bias the study.

b. *Radar data*

The polarimetric Weather Surveillance Radar-1988 Doppler from Weldon Spring Missouri (KLSX) was the primary radar used in this analysis. These data were obtained from the National Center for Environmental Information (NCEI)'s big data project. Radar fields of interest utilized were horizontal reflectivity (Z_h), differential reflectivity (Z_{DR}), correlation coefficient (ρ_{hv}), specific differential phase (K_{DP}), and differential phase (φ_{dp}). In particular, the polarimetric radar data was used to identify times and locations of depolarization streaks due to ice crystal orientation in a strong electric field (e.g., Hendry and McCormick 1976; Krehbiel et al. 1996; Caylor and Chandrasekar 1996; Metcalf 1997; Ryzhkov 2007; Hubbert et al. 2010; Kumjian 2013).

Depolarization streaks are observed in Z_{DR} when the radar is in simultaneous transmit and receive mode (STAR; Doviak et al. 2000; Scott et al. 2001; Ryzhkov and Zrnić 2007). Depolarization streaks can have the appearance of Z_{DR} increasing or decreasing in magnitude along a radial with range because the minor axis of the hydrometeor is not perfectly aligned in the vertical, thus allowing for scattering of both the horizontal and vertical polarization radar signal (Kumjian 2013). Specific differential phase K_{DP} and φ_{dp} are utilized to separate regions with larger aggregates from smaller ice crystals because negative K_{DP} indicates that ice crystals are vertically aligned by electric fields, while Z_{DR} streaks are caused by aggregates and graupel (e.g., Ryzhkov and Zrnić 2007; Kennedy and Rutledge 2011; Kumjian 2013; Thompson et al. 2014; Hubbert and Ellis 2014; Hubbert et al. 2014).

Data from the Level-3 hydrometeor classification algorithm (HCA) from the NCEI radar archive were used to identify the most likely hydrometeors in the region of the lightning activity. These archived data were used to replicate the available information to the NWS forecaster. The algorithm uses fuzzy logic to deduce the most likely hydrometeor present in the radar volume based on the available polarimetric measurements (e.g., Vivekanandan et al. 1999; Straka et al. 2000; Liu and Chandrasekar 2000; Heinselman and Ryzhkov 2006). The algorithm has 10 classification categories, plus an unknown, and a range folded category. Data were displayed using UCAR/Unidata's Integrated Data Viewer (IDV; Unidata 2020). These data are only available up to the 3.4° elevation scan. Even though the Level-3 data are limited in elevation, deduction of the locations of ice crystals/aggregates, graupel, and their proximity to the lightning events examined in this event is beneficial in determining if graupel was potentially identified away from convective cores within the MCS leading line.

c. *Upper air temperature*

Upper air information was obtained from the closest observed sounding at Lincoln, Illinois, at 1400 UTC 20 August

2019. Of key interest was the identification of temperature thresholds of 0°C and −40°C, which provide an estimate on the depth of the mixed phase region and the approximate location of the melting layer. The region from −10° to −15°C is important in determining where charge separation was maximized due to depositional growth of precipitation-sized ice in the presence of supercooled water (Takahashi 1978; Baker and Dash 1994; Saunders et al. 2006; Emersic and Saunders 2010).

d. Lightning risk modeling for IDSS location

Most lightning safety activities focus on the detection of lightning within a certain radius from a point location to communicate the threat to people (e.g., Holle et al. 2016; Schultz et al. 2017; Sanderson et al. 2020; Murphy et al. 2021). Once lightning is observed within a defined radius, there is a stand down period of 10–30 min for outdoor activities, and the variation in time is based on the policies of the end user (e.g., Holle et al. 2016; Schultz et al. 2017; Sanderson et al. 2020). Most of these rules have been developed using point datasets from ground based networks, where spatial information on lightning flashes were not widely available. Schultz et al. (2017) demonstrated that when two-dimensional information about lightning flash size is available, a positive result is an increase in lead time on the first lightning flash at the IDSS location, but also the addition of down time after the threat is over.

Murphy (2018) developed a spatiotemporal risk assessment technique to illustrate the lightning threat for a location of interest. This technique was originally developed using lightning mapping array data (LMA; Rison et al. 1999), but was modified to incorporate spatial information from the GLM instrument. The technique blends components from threat mitigation strategies (e.g., stand down radii) with probabilistic risk calculation from part 2 of the International Electrotechnical Commission Standard (IEC 62305–2). The technique computes lightning risk for a point location using FED within 40 km of that location and local information (i.e., elevation, height of surrounding objects as it relates to human safety). Murphy (2018) and Murphy et al. (2021) have modified the IEC standard from using building heights to incorporating human height in the lightning risk calculation. Only direct strikes are considered in the computation at this time, thus the computation does not account for side flashes or ground current sometimes observed in lightning injury and fatality cases.

For the purposes of this study, the point location selected was the hypothetical IDSS location where the first bolt-from-the-blue CG occurred, and it was assumed that the hypothetical human is out in the open. To model risk to a human at this location, a standard height of a 1.74-m person (5 ft, 7 in.) with a diameter of 0.837 m was utilized as a collection area. Resulting risk was classified into three categories: acceptable, tolerable, and unacceptable. The computed risk values were closely tied to the density of lightning flashes and the range at which flashes were from the decision support location. The risk was computed for 10-min increments to match the minimum stand down period for lightning safety observed by weather enterprise partners (Holle et al. 2016; Stano et al. 2019), and was updated every minute to provide a continuous risk values to determine overall trends for the IDSS location. Ultimately, the purpose of this risk analysis was to provide a tool for forecasters and decision makers to monitor the trend at their location in the event they need to communicate the lightning threat to the general public or to assess when the threat may be trending downward and outdoor activities can resume. For more specific details on the risk calculation and assessment technique, see the appendixes, Murphy (2018) or Murphy et al. (2021).

3. Analysis

a. Environmental overview prior to first flash at IDSS location

The parent convection that generated the large flashes which impacted the hypothetical IDSS location was part of a mesoscale convective system (MCS) that propagated southeastward out of Iowa and Illinois, to Missouri, and Kentucky. A special upper air observation from Lincoln, Illinois (KILX), at 1400 UTC ahead of the MCS indicated surface based convective available potential energy of 1615 J kg^{-1} (Fig. 1). The 0° and −40°C isotherms were located at 4.7 and 10.0 km above ground level, with the −10° and −15°C layer between 6.0 and 6.8 km.

During the 40 min leading up to the lightning event, the closest lightning activity was approximately 30 km to the south of the hypothetical IDSS location across parts of Phelps, Dent, Washington, St. Francois, and Ste. Genevieve Counties (Fig. 2a). Between 2100 and 2140 UTC, zero lightning flashes were observed by NLDN or GLM in Franklin, Jefferson, Warren, or St. Charles Counties in Missouri (Fig. 2b). The closest 30-dBZ echo to the IDSS location at the 0.5° elevation from KLSX during this period was nearly 30 km south in St. Francois County.

b. The initial CG flash outside of surface precipitation

At 2140:15 UTC, a positive ground flash was observed by the NLDN well outside of any precipitation (Fig. 3). This flash was approximately 136 kA, and located in an area that had not observed any lightning in the previous 40 min. This +CG flash was accompanied by five additional IC flash detections and one negative CG flash detection using the NLDN classification algorithms. All seven point detections occurred within 1 s of each other, suggesting that they were likely part of the same lightning event. However, without areal information to connect the NLDN's accurately geolocated points, it was not clear if they were part of the same event. Radar and previous lightning data from the NLDN indicate that there were 2–3 areas from which this flash could propagate within the convective region of the MCS (Fig. 3). The southwest–northeast-oriented NLDN information provides some clue about a southwesterly direction to the flash but it was not fully clear given the points were separated by several km in space, and the timing of the flashes in the NLDN indicates northeast and then southwest propagation.

The GLM Flash Extent Density data product for the same point in time (Figs. 4a,b) reveals from which thunderstorm this

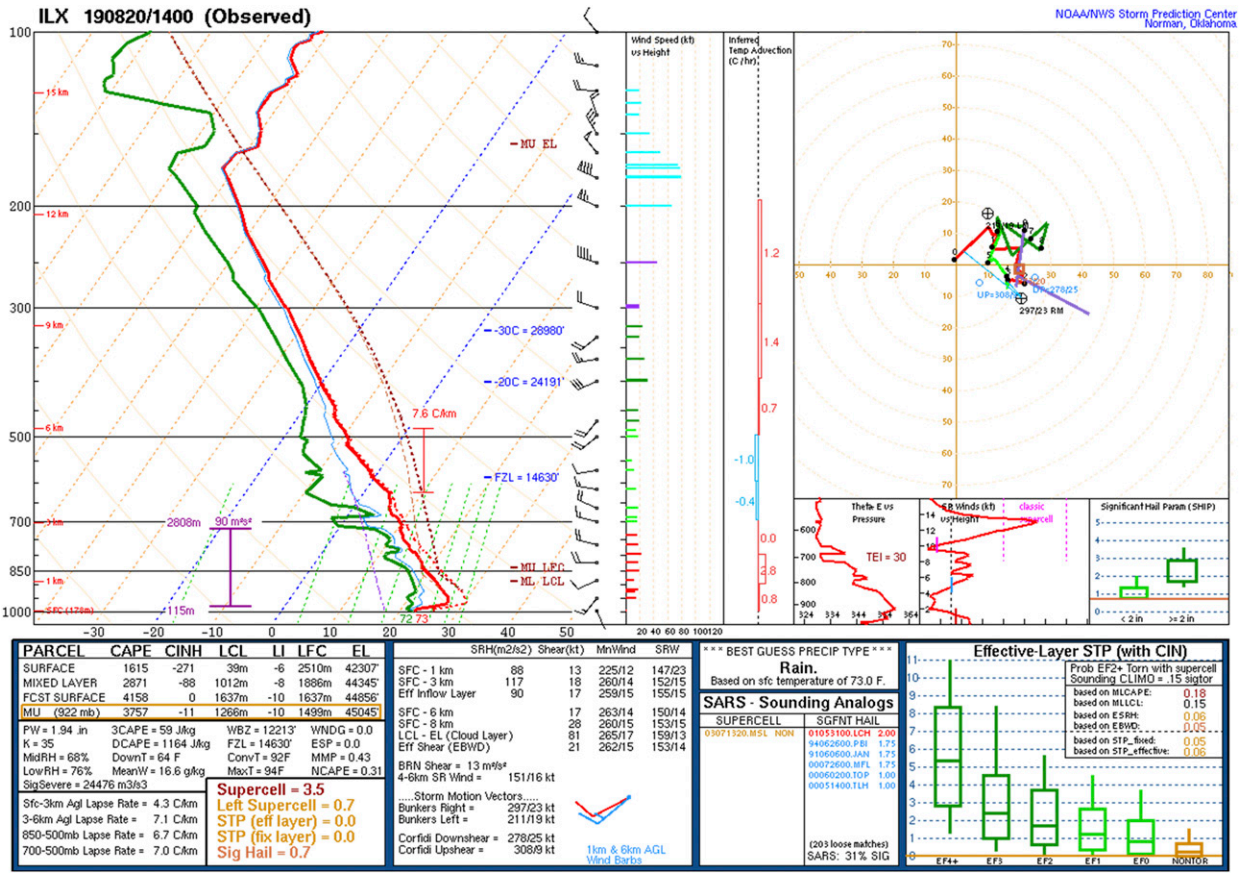

FIG. 1. Observed 1400 UTC upper air sounding from Lincoln, IL (KILX), on 20 Aug 2019.

flash originated. There was a distinct lightning path approximately 75 km long from the thunderstorms to the southwest of the IDSS location over Dent and Phelps Counties in Missouri to the NLDN flash locations in Jefferson and Franklin Counties. A total of four GLM flashes were observed from the Level-2 GLM data. However, using the Peterson (2019) method for recombining GLM groups into reprocessed GLM flashes without the 3-s and 101 group flags, all four Level-2 GLM flashes were combined into one single reprocessed GLM flash. The horizontal area of the flash was approximately 4270 km^2 and its total energy was 6163 fJ. This flash was above the 99th percentile in size and total optical energy when compared to statistical distributions of a full year of data within the Peterson (2019) study. Importantly, the flash came to ground in the absence of surface precipitation (reflectivity was not observed between the 0.5° and 6.4° from KLSX near the IDSS location, and the closest automated observing site had zero precipitation during the previous hour), the parent storm's closest 30-dBZ echo at 0.5° elevation was nearly 75 km away, and the closest precipitation from KLSX was about 30 km to the south of the +CG location and associated with another thunderstorm (Fig. 5a).

A vertical slice of the radar data between the origination point in the MCS convective region and the location where the flash came to ground showed a distinct path of precipitation aloft between 4.7 and 9 km (Fig. 5e). Thus, the lightning traveled within this trailing stratiform region aloft before coming to ground approximately 75 km outside of the closest echo > 30 dBZ at 0.5° elevation from KLSX in the storm that initiated the flash. Areas of enhanced reflectivity were present between 6 and 9 km with values close to 30 dBZ, signifying the presence of ice ≈ 1 mm in diameter (e.g., graupel, aggregates; Fig. 6a). Correlation coefficient (not shown) is uniform in the stratiform region aloft, suggesting that a melting layer was not observed by KLSX at this time and location. Level-3 hydrometeor classification information from KLSX at 2140 UTC indicates that the most likely hydrometeor present were ice crystals and aggregates. These areas of enhanced reflectivity near the melting level have also been observed in anvil clouds that produce ground flashes (e.g., Weiss et al. 2012). The only signals of graupel anywhere near the stratiform flash region were in central St. Francois County, which was approximately 50 km to the southeast of the IDSS location. This region of graupel was directly collocated with a convective core (e.g., Figs. 5a and 6b). Evidence of depolarization streaks along the radials closest to the propagation path were present; however, the signal in Z_{DR} was not as pronounced as the depolarization streaks directly south of the ground flash location (Figs. 5, 7, and 8).

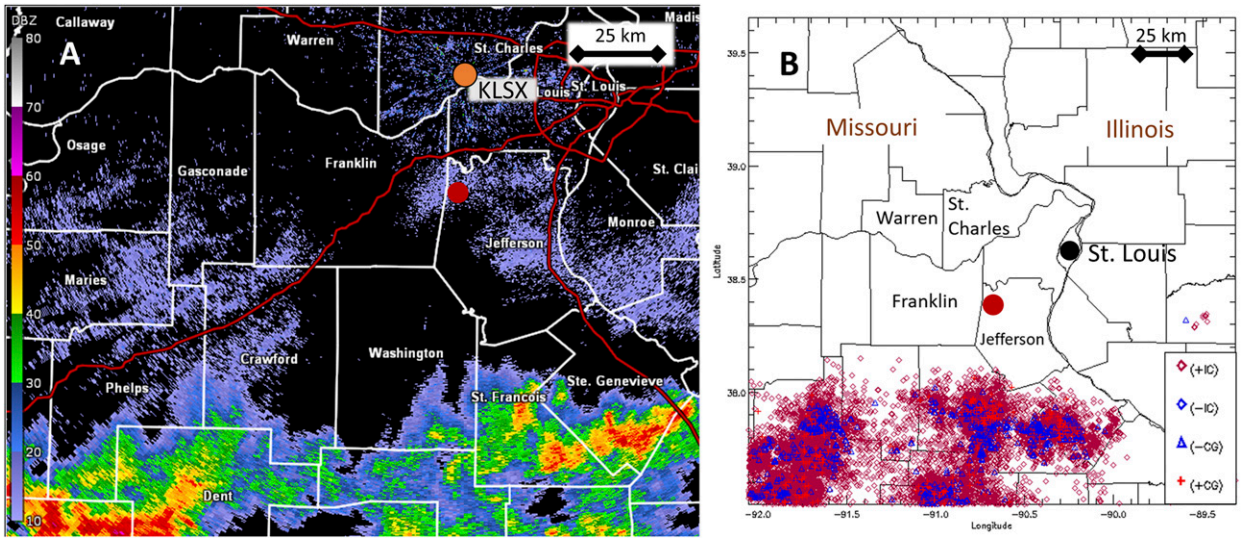

FIG. 2. (a) Reflectivity at 0.4° elevation at 2140 UTC from KLSX (orange dot) in Weldon Spring, MO. (b) NLDN lightning detections between 2100:00 and 2140:00 UTC (1600:00–1640:00 CDT). The red dot is IDSS location where the first CG occurs at 2140:16 UTC. In (b), red diamonds are IC flashes observed by the NLDN, blue triangles are −CG flashes, and red plus signs are +CG flashes.

To expound upon the presence of depolarization streaks, Figs. 7 and 8 depicted Z_{DR} from KLSX between elevations 5.1° and 10.1° at 2135 and 2140 UTC. In Fig. 7, there were up to six radials where there were depolarization streaks present over Phelps, Crawford, Washington, St. Francois, Ste. Genevieve, and Jefferson Counties, Missouri, approximately 30–50 km to the southwest, south, and southeast of the IDSS location. The depolarization streak with the most depth was found over St. Francois and Jefferson Counties, as it was present in all four elevation angles and was in the vicinity of the GLM flash at 2140:15 UTC and the +CG flash. The other five streaks were limited to one or two elevation angles, but they indicated the presence of ice crystals oriented in an electric field in a broad region of the upper levels of the trailing stratiform of the MCS.

c. *Subsequent flashes in the non-precipitating stratiform region*

A total of 12 flashes were observed by GLM between 2145 and 2222 UTC where GLM flash extent density was within 40 km of the hypothetical IDSS location. The average size of these 12 flashes was 3184 km^2, and an average total optical

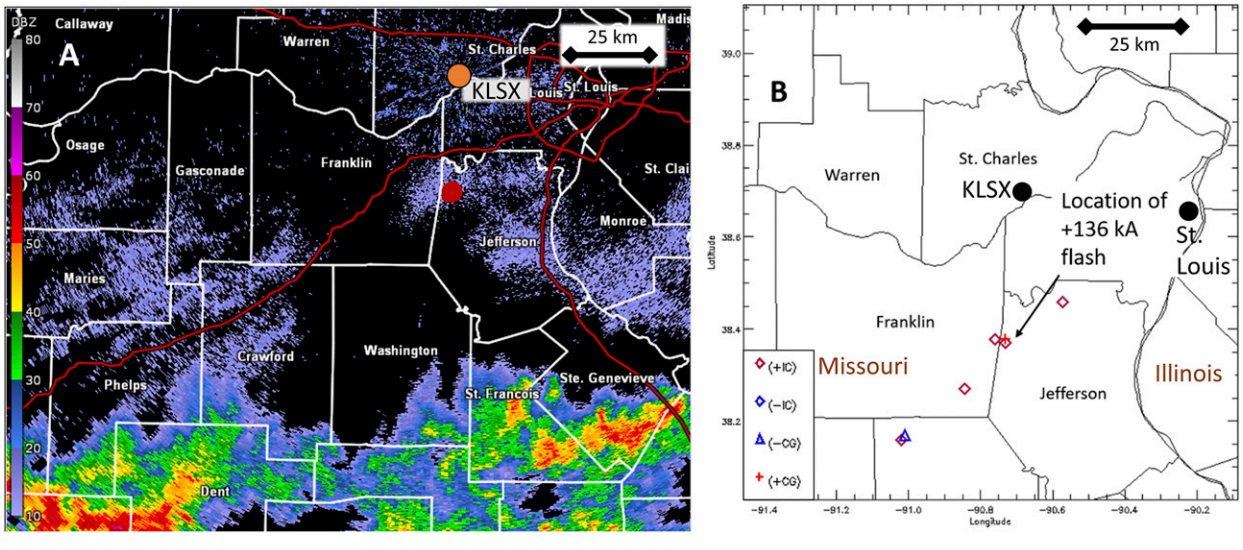

FIG. 3. (a) Radar reflectivity at 0.4° elevation at 2140 UTC from KLSX (orange dot) in Weldon Spring, MO. (b) NLDN lightning detections between 2140:15 and 2140:16 UTC. In (b), red diamonds are IC flashes observed by the NLDN, blue triangles are −CG flashes, and red plus signs are +CG flashes. The red dot in (a) corresponds to the +136-kA flash location in (b).

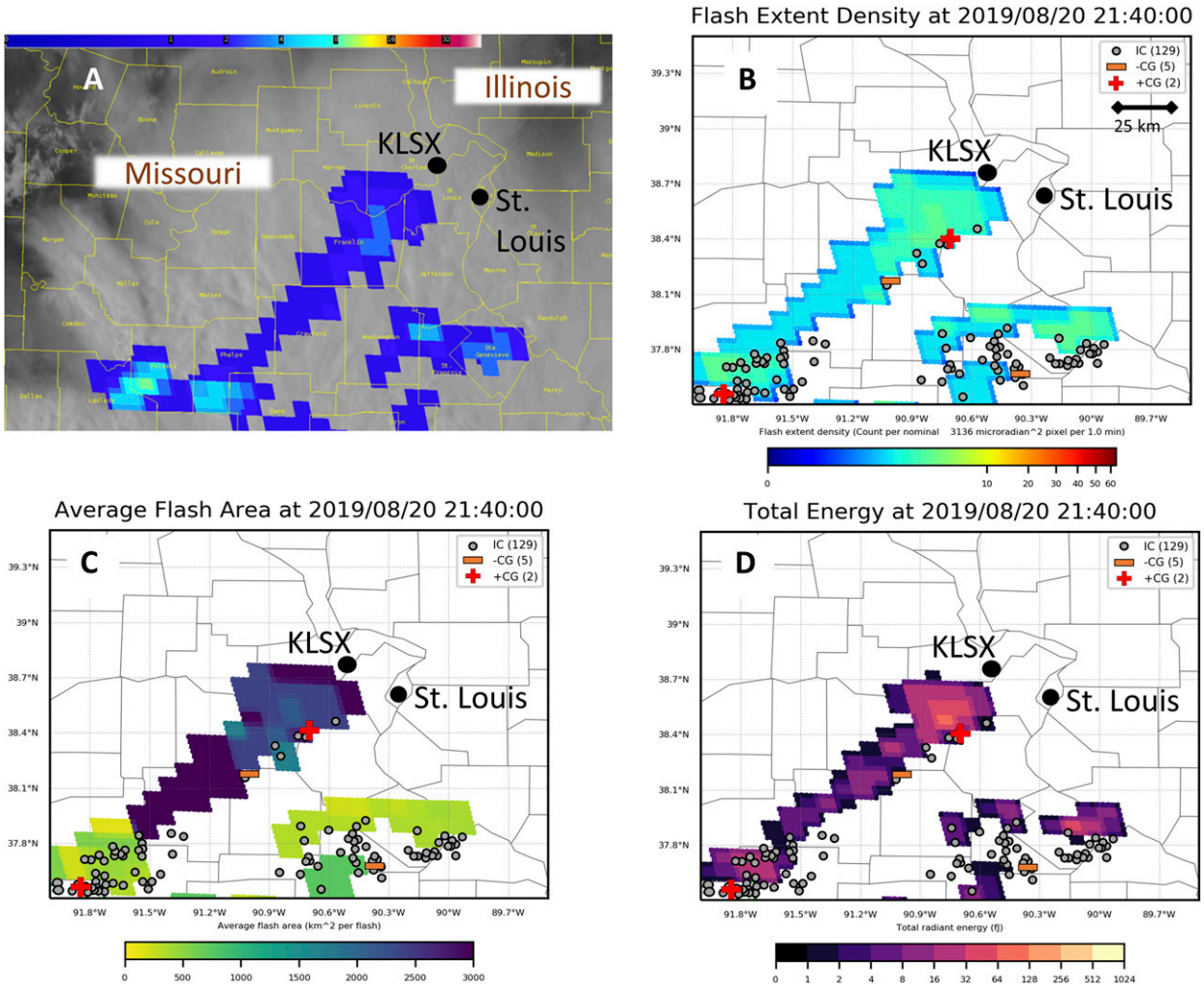

FIG. 4. (a) GOES GLM flash extent density overlaid on 0.64-μm ABI data at 2140 UTC (1640 CDT) using AWPS2 over east-central MO and southwest IL. (b) GLM flash extent density using GLM tools. (c) The average flash area (km^2). (d) GLM total optical energy (fJ). NLDN lightning flashes are overlaid on (b) and (d), where red plus signs are the location of +CG, orange minus signs are the location of −CG, and gray dots are the location of IC flashes.

energy of 7734 fJ. The NLDN identified 34 flash locations within this 40-km radius during this period (Table 1). In total, seven CG flashes were observed within 40 km of the hypothesized IDSS location. Two of these CG flashes were positive and the other five were negative polarity. Four of the seven ground locations were coincident with two GLM flashes (2150 UTC and 2153 UTC; Fig. 9). Only one of these additional CG flashes fell within 15 km of the first location. That was an 80-kA +CG flash at 2153:26 UTC, located 13 km to the south-southeast of the IDSS location. Upon further inspection of the data, two of the −CG flashes associated with flashes at 2150 and 2153 UTC were −3 and −5 kA, respectively, which was possibly a misclassification of lightning type by the NLDN (e.g., Biagi et al. 2007; Fleenor et al. 2009; Cummins and Murphy 2009). In total, 6 of the 12 additional flashes observed by GLM within the 40-km radius did not have any observed CG activity from the NLDN within the 40-km radius. Each of these flashes propagated through a region where depolarization streaks were present just before lightning occurrence between 2145 and 2150 UTC (Figs. 9e,f).

One flash at 2210:35 UTC produced flashes of both polarity during propagation (Fig. 10). A +99-kA +CG and a two stroke −CG with a peak amplitude of −21 kA were observed within a second of each other along the Jefferson County and St. Francois County line. This −CG flash was 21 km from the IDSS location, while the positive flash fell just outside of the 40-km radius for the flash location. The most interesting feature of this flash was the channel like structure that was apparent in the total optical energy field to the southeast of the CG flash locations (Fig. 10b). Much of this region was above 128 fJ km^{-2} and there appeared to be a continuous "L" shape in the TOE field surrounded by lower brightness values. It is hypothesized that these brighter areas were indicative of channels within the flash. This flash propagated right through

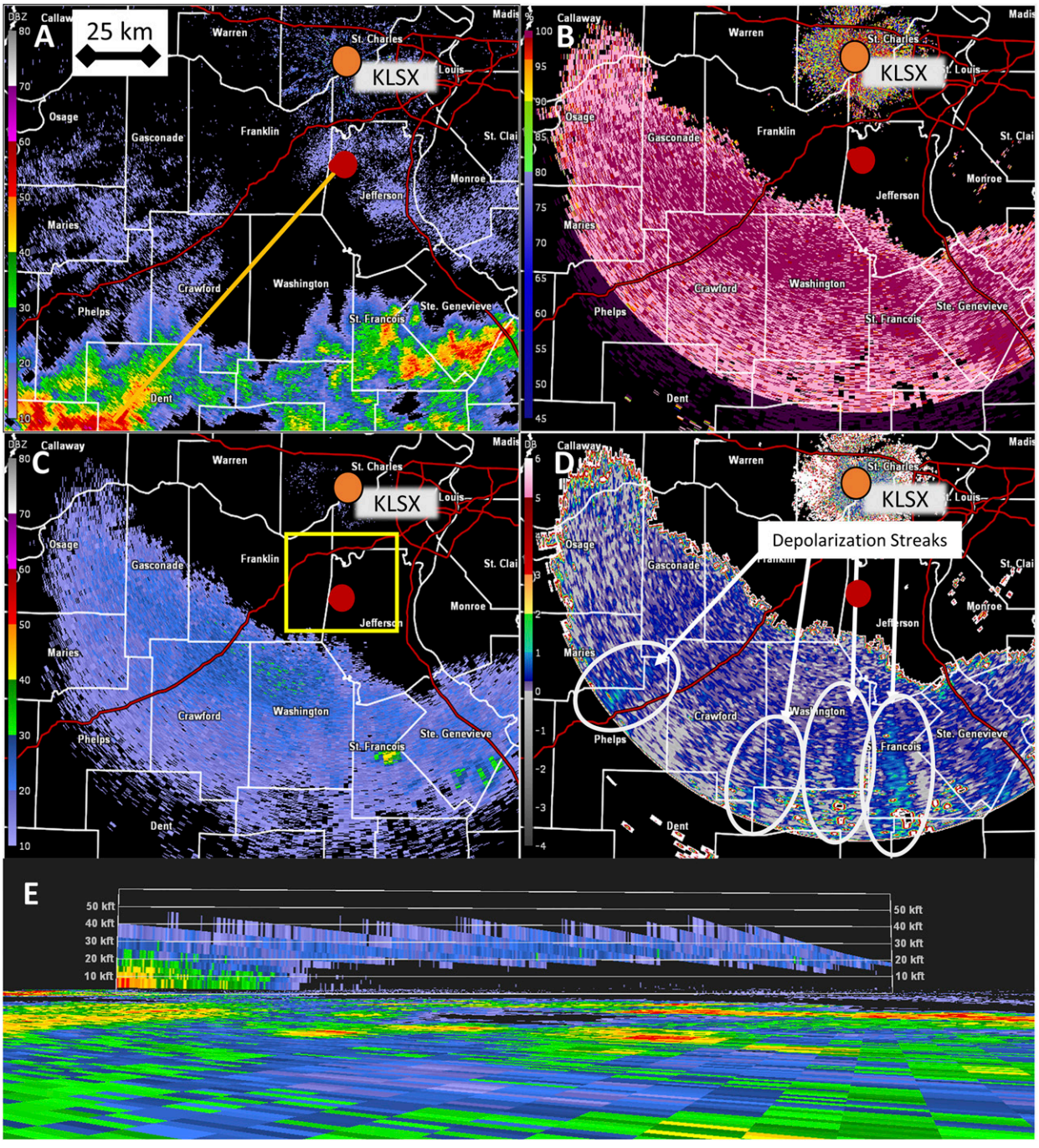

FIG. 5. Five panel radar display at 2140 UTC from KLSX (orange dot). (a) Horizontal reflectivity at 0.5°, (b) correlation coefficient at 6.4°, (c) horizontal reflectivity at 6.4°, (d) differential reflectivity at 6.4°, and (e) a vertical cross section of reflectivity along the orange line in (a). Depolarization streaks in (d) are identified by white ovals and white arrows, and the red dot indicates the location of the +136 kA CG location. The yellow box indicates the location of (b) in Fig. 6.

regions over Washington County and St. Francois County where multiple depolarization streaks were present in the 4.0° and 5.1° elevation angles from KLSX. The enhancement in reflectivity remained near the melting layer, and both CG locations occurred below this region of enhanced reflectivity (Fig. 11).

d. *Lightning risk model from the perspective of the first CG location*

In the 40 min leading up to the first CG flash, risk assessment using GLM data initially showed a decreasing trend in lightning risk as the parent MCS moved southward from

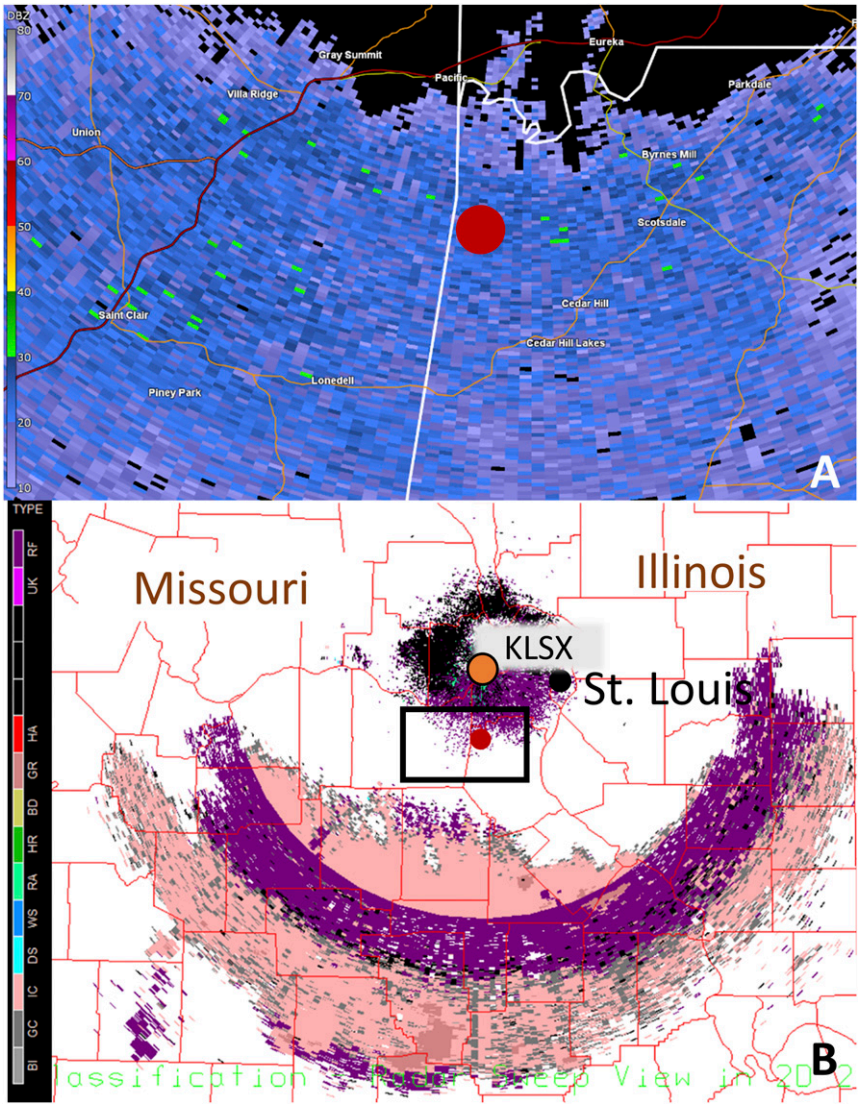

FIG. 6. (a) Reflectivity at 10.1° elevation from the same radar volume. (b) Level-3 hydrometeor classification from KLSX (orange dot) at 2135 UTC 20 Aug 2019. The red dot indicates the hypothetical IDSS location. The black rectangle in (b) is the approximate domain for (a).

the hypothetical IDSS location (Fig. 12). The risk between 2100 and 2130 UTC diminished from unacceptable to tolerable as flashes moved outside of the 15-km range ring from the IDSS location. At 2140 UTC, the risk trended upward toward the tolerable/unacceptable line as the spatial extent of the first stratiform flash was observed by GLM enters the 40-km buffer around the IDSS location (Fig. 12, blue star). With each of the 12 additional flashes, there were small increases in the risk. The risk model did not return to the unacceptable range until 2150 UTC when subsequent lightning flashes observed by GLM occurred in the 40-km radius around the IDSS location. The lightning risk at the IDSS location remained above the unacceptable range through 2203 UTC. The last flash to impact the 15-km inner safety radius of the IDSS location occurred at 2210 UTC, and the second largest increase in the calculated lightning risk from the model is observed. Then by 2221 UTC, the risk dramatically dropped from near the tolerable/unacceptable line down toward the broadly acceptable line as the flash from 2210 UTC that went right over the IDSS location aged out of the risk computation. A second large drop occurred at 2228 UTC when the flash at 2217 UTC aged off in the calculation. The 2217 UTC flash was the last to touch the 15-km range ring. After 2227 UTC, the lightning risk hovered between the broadly acceptable and tolerable region as flashes at 2236 and 2248 UTC briefly skirted the outer 40-km range ring consequently causing nonzero risk for a period of 10 min following.

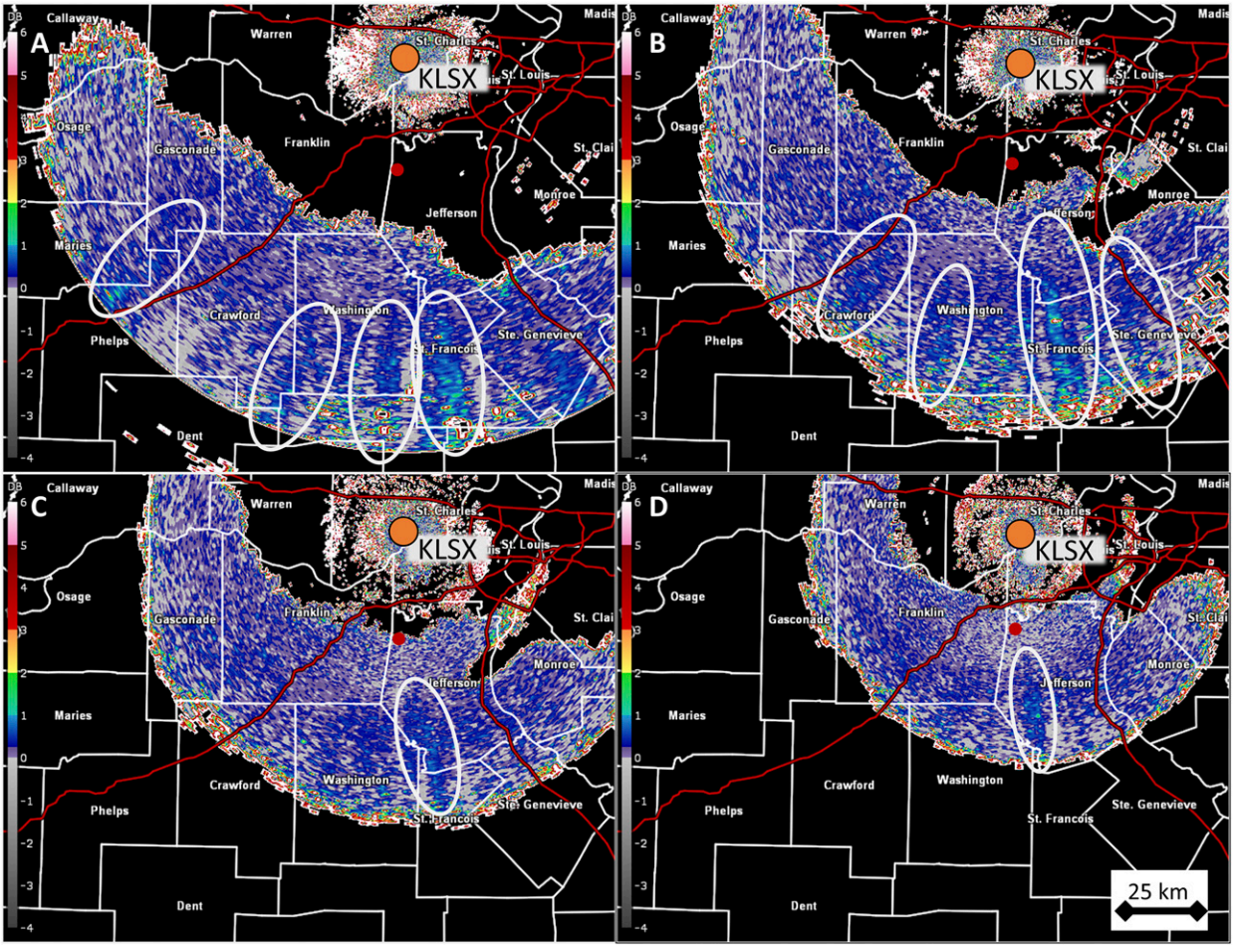

FIG. 7. This is a four panel spread of differential reflectivity Z_{DR} from KLSX (orange dot) at 2135 UTC: (a) elevation 5.1°, (b) radar elevation 6.4°, (c) elevation 8.0°, and (d) elevation 10.1°. The red dot corresponds to the location of the first bolt from the blue flash at 2140:16 UTC. The white ovals indicate the locations of depolarization streaks in Z_{DR}.

4. Discussion

a. Lightning data fusion

Fusion of GLM and NLDN lightning data provide a unique picture of these large lightning events because one can capitalize on the strengths of both systems. The NLDN provides specific point location of ground flashes. It also may provide some information regarding the storm charge structure as inferred from the polarity of the ground flashes. The GLM provides areal coverage of the flash and the intensity of the light that escapes cloud top. When combined, decision makers can see the areal extent of the parent flash, and each location where the same flash came to ground.

Parallax will naturally occur between these datasets because they are geolocating lightning information at two different levels (cloud top from GLM versus at the surface with NLDN or ENTLN). Additional parallax issues will occur with increasing latitude just like with advanced baseline imager ABI information. The forecaster can account for these differences by assuming that the NLDN (or ENTLN) data will be located more equatorward than the GLM data and ground impacts from lightning will be most prevalent near these point locations. This is most prevalent in Fig. 4, where the NLDN information is located along the southeastern periphery of the mapped GLM information. NLDN identifies the locations impacted at the ground, while GLM indicates where the flash originated.

b. WFO forecast desk perspective

The NWS forecast office in St. Louis frequently provides decision support to core partner outdoor events. For many of these partners, lightning is a primary concern and NWS St. Louis strives to provide advance notice of potential lightning activity. From the perspective of a forecaster providing support to these events, the fusion of the datasets is key. The NLDN, ENTLN, and GLM are used extensively to identify electrified storms approaching IDSS events. Given that IC lightning activity typically precedes cloud-to-ground strikes (MacGorman et al. 2011; Schultz et al. 2017), NWS St. Louis preferentially utilizes networks that efficiently detect IC flashes (e.g., ENTLN,

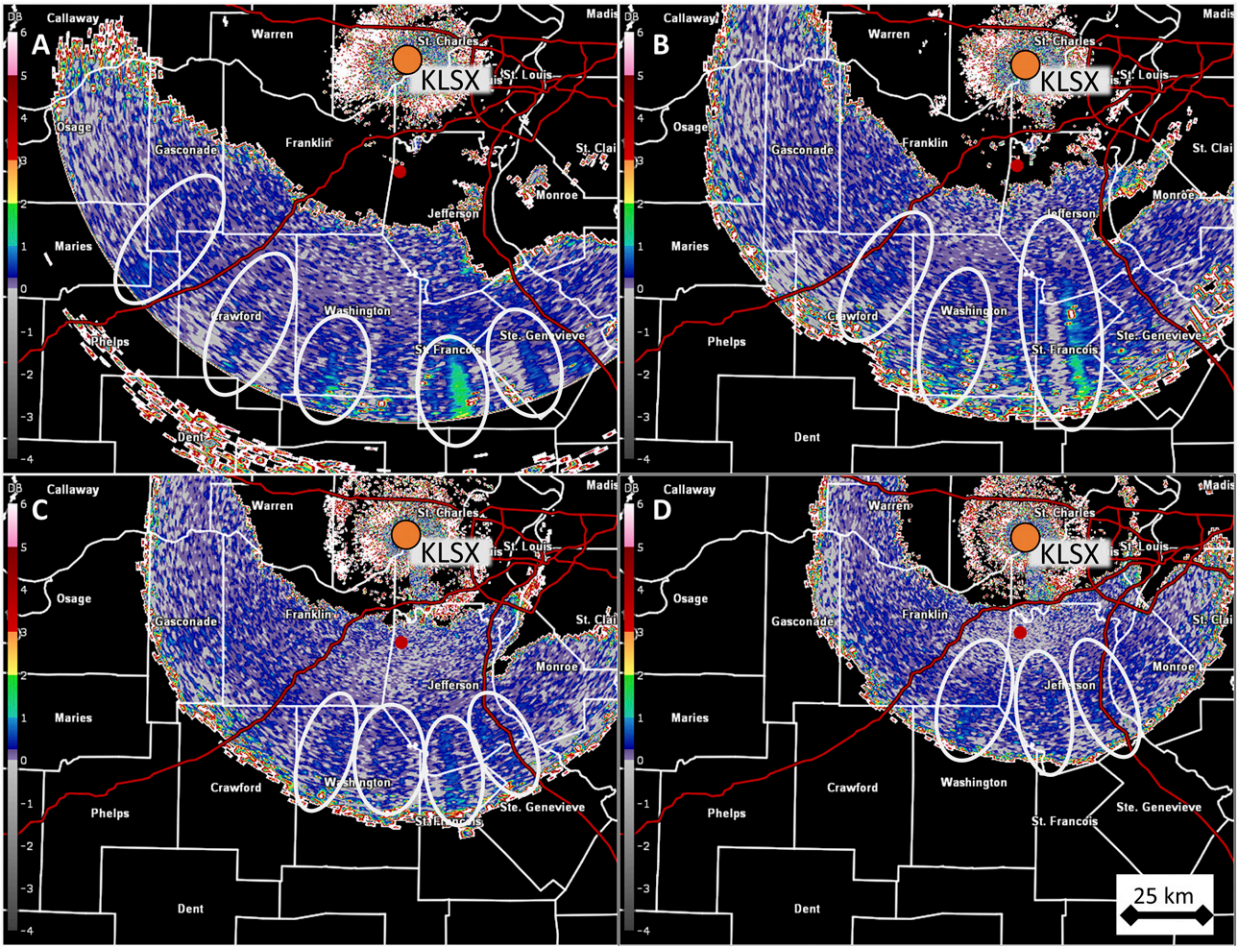

FIG. 8. As in Fig. 7, but for 2140 UTC from KLSX.

GLM) to get lead time on CG strikes, and relies heavily on the NLDN to identify CG activity and locations.[2] If a forecaster observes any lightning approaching an IDSS event, a prompt call to the partner is made to communicate the threat. In cases where storms are traversing the CWA, NWS St. Louis aims for 1-h lead time. While the St. Louis WFO did not have any specific IDSS events in the area at the time, in hindsight blending the radar, satellite, and lightning information is a best practice for generalized decision support for partners through NWSChat (a collaborative chat program used by NWS forecasters) or to the public through social media.

Outside of the lightning detection networks, the St. Louis WFO relies on radar and a handful of *GOES-16* red, green, blue (RGB) imagery. In particular, the Day Cloud Convection or Day Cloud Phase products are used in a similar manner to Elsenheimer and Gravelle (2019), especially prior to flash initiation. For an event like this, it seems that the radar signatures are the more useful indicators for identification of the electrified cloud because glaciation has already occurred. Given the broad mesoscale precipitation, slower rates of charging in the trailing stratiform region of the MCS, and infrequency of the flashes, the depolarization signatures are detectable because the precipitation are not rapidly changing orientation. This made it possible to observe the orientation of the ice within the cloud using Z_{DR}. Closer to the convective core, the challenge is that the local electric field is changing far faster than the scanning strategy of the radar due to the increased charging rates, complexity of charge structure, and the nearly constant lightning flash rates near the region of the storm updraft (e.g., Bruning and MacGorman 2013). Also, parts of the storm near the convective cores can also contain larger liquid hydrometeors that have been lofted above the freezing level (e.g., Z_{DR} columns) which contaminate the signal. Thus, the depolarization streaks are not as easily discernable in convective regions of thunderstorms because the signal too rapid for the current operational network of radars. However, future phased array radar capabilities may provide the ability to observe these rapid changes closer to the convective cores.

[2] At the time the present study was generated, the NWS only received CG information from the NLDN into their AWIPS system. Work was being undertaken to incorporate IC information from Vaisala lightning sensors.

TABLE 1. The 1-min time frames in AWIPS2 where large lightning events were noted trailing the main convection and within 40 km of the hypothesized IDSS location at 38.378°, −98.730°.

Time (UTC)	No. of L2 GLM flashes	Peterson method GLM flashes	Total size (km^2)	Total energy (fJ)	No. of NLDN points	No. of NLDN within 40 km	IC within 40 km	CG within 40 km
2140	4	1	4270	6163	8	8	6	2
2145	1	1	907	731	2	0	0	0
2150	4	2	4827	14 349	22	17	15	2
2153	2	1	3284	6377	8	7	5	2
2157	2	2	2982	7131	2	1	1	0
2200	2	1	3485	9760	0	0	0	0
2210	8	1	10 473	34 689	7	1	0	1
2217	2	1	3270	5379	16	0	0	0
2220	2	1	2902	7334	10	0	0	0
2222	5	2	4990	8624	0	0	0	0
Sum/avg	32	13	3184	7734	75	34	27	7

c. *Implications for lightning safety*

Large bolt from the blue events have been reported in the literature previously (e.g., Kuhlman et al. 2009; Weiss et al. 2012; Fuelberg et al. 2014). This event challenges current lightning safety protocols because any lightning safety protocols would not have been in place for the IDSS location at the hypothesized IDSS location due to the absence of lightning within 10 km during the previous 30 min (Holle et al. 2016; Stano et al. 2019). Once lightning was observed over the IDSS location, the standard 30-min safety protocol would have remained in effect until 2247 UTC because the last GLM flash to encroach on the 15-km range ring occurred at 2217 UTC. If solely going by the NLDN information, the last flash to affect the IDSS location was at 2153 UTC, meaning the 30 min would have expired at 2223 UTC. Schultz et al. (2017) noted that additional downtime was incurred when using two-dimensional information on lightning for safety as compared to solely using the NLDN. It is worth noting that the flashes at 2157, 2200, and 2210 UTC were all within 5 km of the IDSS location, with the flash at 2210 UTC propagating directly over the IDSS spot.

Trends in the lightning risk model prior to 2140 UTC also indicated that the lightning threat diminished for the IDSS location. However, once the bolt from the blue event occurred, subsequent lightning flashes contributed to an increase in the risk category, which ultimately pushed the threat above the unacceptable risk category. This case also reveals that the infrequent nature of these flashes can pose a challenge to the model because in this case, at least three flashes were needed inside the 15-km range ring in a 10-min period to bump the risk to the unacceptable range. In comparison with the standard 30-min lightning protocols from the perspective of GLM, the risk model could have potentially provided enough information to end the stand down period 10 min earlier; however, more work needs to be done. The model's behavior in a variety of storm types and with different operational uses must be undertaken to make sure that the use of the model does not put people needlessly at risk.

d. *Utilization of radar data to anticipate infrequent lightning*

The main indicator of electrification in this part of the stratiform region prior to lightning occurrence was the presence of depolarization streaks above the freezing level. As Kumjian (2013) noted, not every depolarization streak will result in lightning and more examples must be examined to quantify frequency and application of these polarimetric artifacts to IDSS. Application seems to be most operationally feasible in stratiform (e.g., Schultz and Carcione 2020), anvil, or winter weather situations (e.g., Kumjian and Deierling 2015) because of slower charging rates and larger breakdown field needed to initiate the flash (Takahashi 1978; Saunders et al. 2006; Bruning and MacGorman 2013).

An important observation from this case was that this flash's propagation path from the convective region to the final CG location was not along the radials with the largest magnitude depolarization streaks. It is not clear at this time why this was the case, but it does demonstrate that magnitude of the depolarization streak may not matter as much as the *presence* of one. The radial spread of multiple depolarization streaks may be a first-order approximation of the areal extent of the electrified region with the potential for lightning given the alignment between the depolarization streaks and both lightning datasets presented in Figs. 5 and 7–10.

Another possible indicator of electrification and CG potential was the presence of enhanced reflectivity near the melting level (Figs. 5, 6, and 11). In their study of CG lightning beneath anvil clouds, Weiss et al. (2012) noted that in some storms the presence of a reflectivity maximum in the anvil cloud corresponded to where IC flashes initiated and where CG flashes came to ground beneath the anvil cloud. Weak updrafts in the stratiform regions of MCS's have been observed to contain a combination of small graupel and liquid water (e.g., Zrnić et al. 1993) and both aggregation and riming processes have been observed in combination near the melting level in enhanced reflectivity regions in stratiform precipitation (e.g., Giangrande et al. 2016). Thus, it is possible that graupel may have been present, but not identified as the primary hydrometeor in the MCS stratiform region in which these flashes developed. Therefore, both charge advection and in situ charging mechanisms potentially contributed to the development of the strong electric field in the MCS stratiform, which

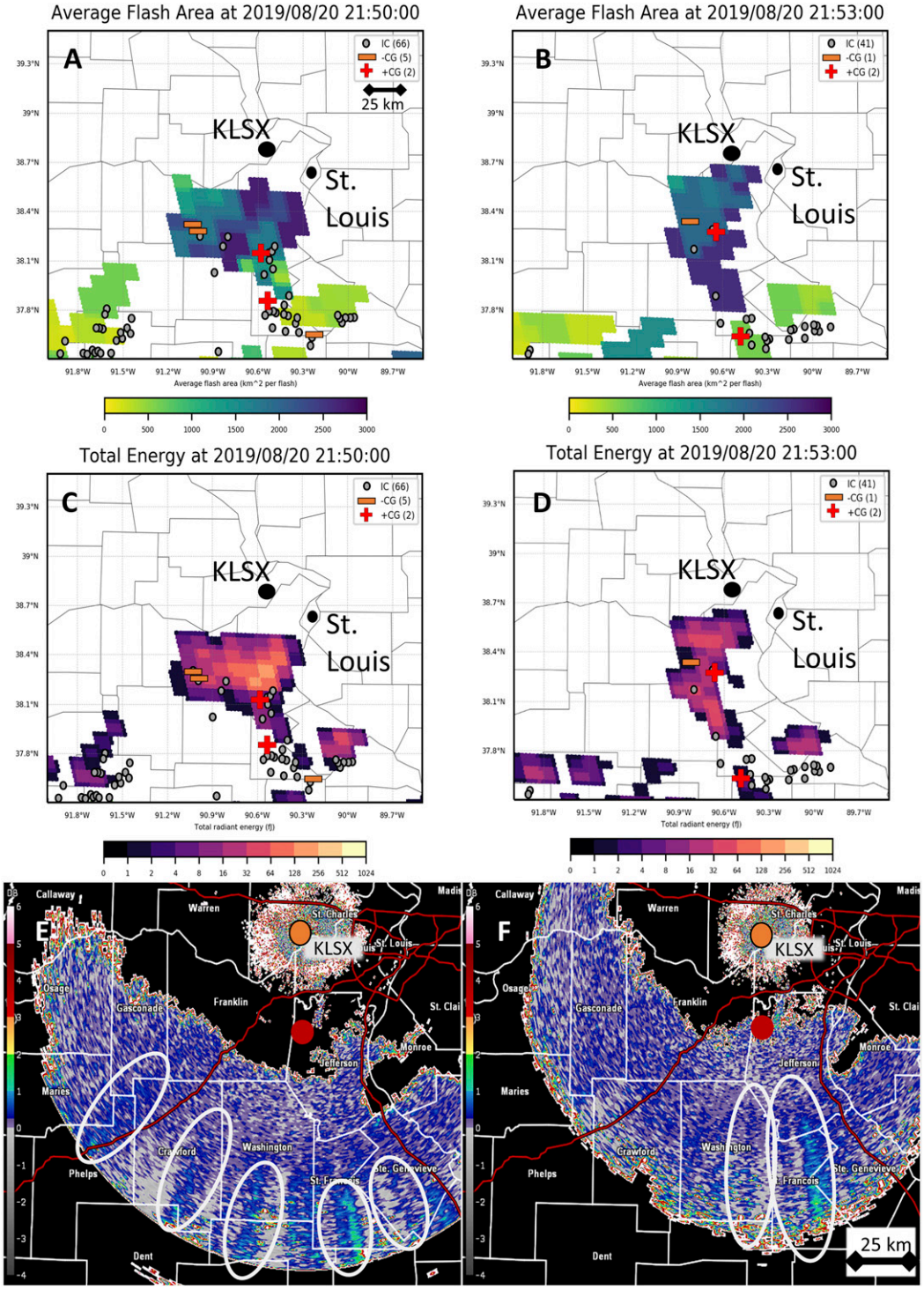

FIG. 9. GLM and NLDN flashes at (a),(c) 2150 UTC and (b),(d) 2153 UTC over east-central MO and southwest IL. (top) Average flash area and (middle) total optical energy. Red plus signs are the location of +CG, orange minus signs are the location of −CGs, and gray dots are the location of IC flashes. (e),(f) Z_{DR} at 5.1° and 6.4° elevation from KLSX (orange dot) at 2145 UTC 20 Aug 2019.

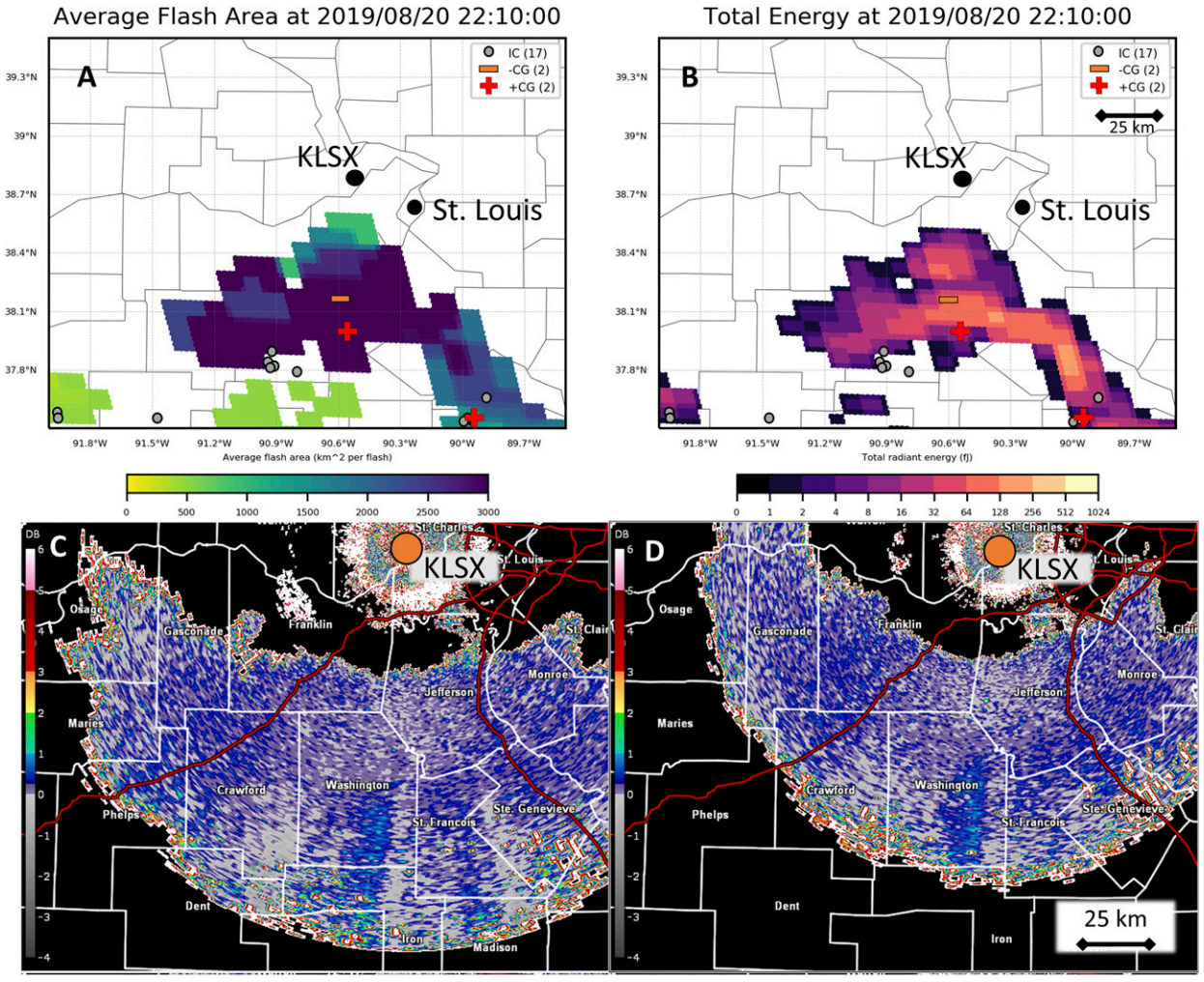

FIG. 10. Four panel image of flashes at 2210 UTC over east-central MO and southwest IL. (a) Average flash area and (b) total optical energy. Red plus signs are the location of +CG, orange/brown minus signs are the location of −CG, and gray dots are the location of IC flashes. (c),(d) Z_{DR} at 4.0° and 5.1° elevation at 2205 UTC from KLSX (orange dot).

in turn resulted in long flash propagation and CG lightning activity outside of surface precipitation.

5. Conclusions

This paper analyzed an event from 20 August 2019 in the NWS St. Louis CWA from the perspective of IDSS decision making and the challenges that can occur with infrequent flashes and bolts-from-the-blue. This analysis complemented the work of Elsenheimer and Gravelle (2019) to provide a holistic examination of lightning threats during growth and decay of thunderstorms, where the majority of people are injured or killed. GLM, NLDN, and radar information were combined to assess the storm environment in which these flashes developed and produced multiple ground flashes in non-precipitating stratiform. Furthermore, two independent lightning datasets were combined to provide spatial information on the lightning event to identify its source convection, and identify where the lightning flash came to ground. Findings include the following:

1) A total of 13 GLM flashes in a non-precipitating stratiform region were observed between 2100 and 2300 over east-central Missouri. The mean flash size was 3184 km^2, and the average total optical energy was 7734 fJ, which is above the 99th percentile for GLM flash size and total optical energy reported in Peterson (2019).
2) A total of 75 NLDN flash points were located within these 13 GLM flashes. A total of 34 of these flashes fell within 40 km of the hypothetical IDSS location, with 9 of them occurring within 15 km of the hypothetical IDSS location. In total, 7 of these 34 flashes came to ground, and 3 of these were strong +CG flashes with peak amplitudes above 80 kA. All eight flashes fell more than 10 km outside of precipitation. An average of 5.8 NLDN flashes were coincident with the 13 observed GLM flashes. Two GLM flashes did not contain NLDN flash identifiers.

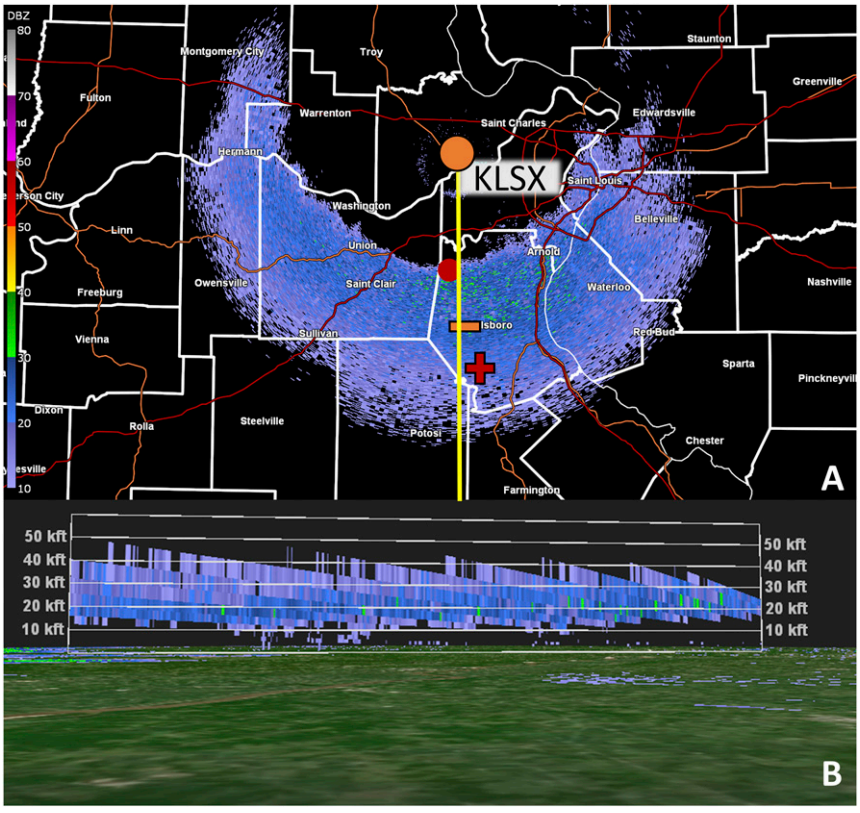

FIG. 11. (a) Reflectivity at 10.1° elevation from KLSX (orange dot) at 2205 UTC, and (b) a cross section of reflectivity along the white line in (a). The red dot is the IDSS location, the orange minus is the location of the −CG flash, and the plus sign is the location of the +CG flash at 2210:35 UTC. The yellow line is the cross section location for (b).

3) The only indications of electrification prior to the first bolt from the blue flashes were depolarization streaks in Z_{DR} within the mixed phase region of the trailing stratiform precipitation and enhancements in reflectivity near the melting layer. It is not clear at this point in time how frequently depolarization streak presence or enhancements in the melting layer results in lightning; however, the observed GLM flashes that resulted in bolts from the blue during this period emanated from radials where depolarization streaks in Z_{DR} were present.
4) Lightning safety protocols would not have been in place prior to the flash observed from this non-precipitating stratiform region. For this case, the lightning risk model used in Murphy et al. (2021) would have indicated the lightning risk was tolerable, but not unacceptable until three of these large lightning flashes entered the 15-km warning radius for the hypothetical IDSS location at 2150 UTC.

This combination of datasets is one potential way to move lightning IDSS beyond reacting to lightning occurrence. Providing meteorological context in anticipation of lightning potential should lead to greater awareness of the hazard and greater lightning risk lead times. This work also fosters the continued transition of lightning safety to incorporate two-dimensional lightning information with traditionally used metrics for in the GLM-era to enhance lightning safety protocols and messaging. This case also provides a challenge to current deep learning methods in development to predict CG occurrence because the CG locations were well removed from the convective elements that initiated the flash. Future work needs to quantify the use of this combined lightning and radar dataset to understand the feasibility of the approach and how it can be implemented operationally for anticipation of infrequent lightning propagation in stratiform or anvil regions of storms.

Acknowledgments. Team members Schultz, Murphy, and Ringhausen would like to acknowledge the support of the GOES-R Proving Ground, namely Dr. Dan Lindsey, Dr. Steve Goodman, and Dr. Scott Rudlosky under Grants NA16AANEG0091 and NA16OAR4320199. Allen would like to acknowledge partial support by NASA Science Mission Directorate's Weather Focus area under the direction of Dr. Tsengdar Lee. Team member Weiss acknowledges support from NASA 80NSSC19K1576 to perform this work. The team also appreciates the additional review of the draft manuscript from Mr. Brian Carcione and Mr. Kris White from the NWS Huntsville Weather Forecast Office. Author Schultz is appreciative of conversations with Dr. Matthew Kumjian and

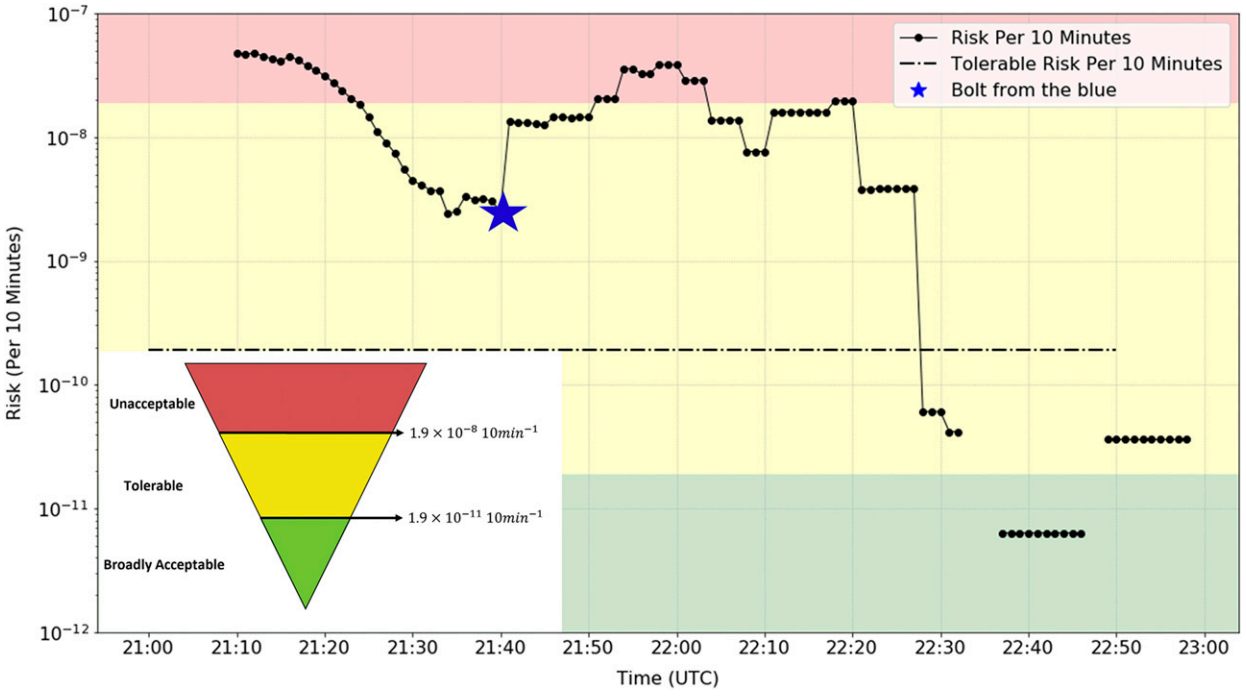

FIG. 12. The 10-min accumulated lightning risk between 2100 and 2300 UTC. The risk is updated every 1 min at the hypothetical IDSS location of 38.378°, −90.730°. The red shaded area indicates unacceptable lightning risk, the yellow shaded area indicates a tolerable lightning risk, and the green area indicates an acceptable risk. The blue star denotes the time of the first bolt from the blue lightning flash.

Mr. Joey Picca on the application of depolarization streaks in real time that inspired this fusion with the lightning datasets for IDSS applications. NLDN lightning data are available through Vaisala Inc. and the Global Hydrology Resource Center (https://ghrc.nsstc.nasa.gov/home/). Both GLM and radar data used in this study are available through the National Centers for Environmental Information's Amazon Web Services: https://registry.opendata.aws/noaa-goes/, https://www.ncdc.noaa.gov/data-access/radar-data/noaa-big-data-project. Finally the authors would like to recognize the efforts of three anonymous reviewers who helped considerably in the revision of this manuscript to improve clarity and reproducibility of the study.

APPENDIX A

Part I: Risk Calculation

The risk calculation used in this analysis is based on the guidelines from the IEC 62305–2, which specifically looks at lightning risk to buildings and structures (International Electrotechnical Commission 2010). The calculation is modified to be applicable to this research by considering humans instead of structures, and assumes lightning strikes at their location, which can cause injury by electric shock (calculated by R_A) or physical damage (calculated by R_B). Total risk R_T of loss of human life is then found by calculating the sum of the risk components (R_A and R_B):

$$R_T = R_A + R_B. \tag{A1}$$

These risk components are solved using Eqs. (A2) and (A3):

$$R_A = N_D \times P_A \times L_A, \tag{A2}$$

$$R_B = N_D \times P_B \times L_B. \tag{A3}$$

The components are the product of the number of dangerous events per unit time (N_D), a probability of damage (P_A or P_B), and consequent loss (L_A or L_B).

a. Number of dangerous events

To solve for N_D [Eq. (A4)] requires a collection area A_D, the density of lightning flashes N_G, and a location factor C_D (that accounts for the surroundings of the person at risk) selected from a lookup table from the IEC 62305–2 standard:

$$N_D = N_G \times A_D \times C_D \times 10^{-6}. \tag{A4}$$

Here, N_G is computed in the 2 km × 2 km ABI grid spacing generated by GLM tools. A Gaussian distribution filter [Eq. (A5)] was applied to the lightning appearing within a 40-km radius R as described in the equation below, where r is distance away from the hypothetical IDSS location, 38.378°, −90.730° (bolt from the blue flash), and $\alpha = 2$ in order to allow for lightning occurring on the outer edge of the radius to contribute to N_G. This filter allows lightning closer to the center of the radius to contribute more to the risk than those that are further away:

$$\text{fgauss} = \exp\left[-\frac{1}{2}\left(\alpha\frac{r}{R}\right)^2\right]. \quad \text{(A5)}$$

The collection area A_D is computed using measurements of a human being (1.74 m high × 0.837 m long × 0.837 m wide). The value for C_D is assigned a value of 1 from the IEC 62305–2 standard to represent an isolated/human. The collection area is computed as

$$A_D = L \times W + 2 \times (3 \times H) \times (L + W) + \times (3 \times H)^2. \quad \text{(A6)}$$

b. Probability of damage

To solve for the probability of damage (P_A and P_B) involves the consideration of protection measures in place. It is assumed none are present for this research, which assigns a value of 1 for both P_A and P_B.

c. Consequent loss

Consequent loss for both components is found through the use of Eqs. (A7) and (A8):

$$L_A = \text{rt} \times \text{LT} \times (\text{nZ/nt}) \times (\text{tz/8760 h}), \quad \text{(A7)}$$

$$L_B = \text{rp} \times \text{rf} \times \text{hz} \times \text{LF} \times (\text{nZ/nt}) \times (\text{tz/8760 h}). \quad \text{(A8)}$$

For L_A, the terms rt and LT are given a value based on look-up tables in IEC 62305–2. The term rt is a reduction factor based upon the type of floor or soil in the location; it is assigned 10^{-2} in this paper to indicate an individual standing on an agricultural surface. LT is the typical mean relative numbers of victims injured by due to one dangerous event and is assigned 10^{-2}. The variables nZ and nt are both assigned a value of 1 to indicate the number of people (nt) in a specific zone (nZ; for this research we consider only one zone—the point location). For the final term in Eq. (A7), tz is the time exposed and the denominator is modified to represent the time over which risk is calculated (10 min). We assumed the hypothetical individual at risk to always be exposed from 2100 to 2300 UTC, so this last term is set to equal 1 (10 min/10 min = 1).

For L_B, the last two terms are identical to L_A. The first four terms are as follows: rp is assigned a value of 1 to indicate no provisions are taken in the event of consequences of fire, rf is assigned a value of 10^{-2} to indicate an ordinary risk of fire, hz is assigned a value of 1 to indicate no special hazards present, and LF is the typical mean relative numbers of victims by physical damage due to one dangerous event and assigned value of 10^{-2}.

APPENDIX B

Part II: Risk Assessment

Calculated risk values are evaluated based upon tolerance thresholds defined by the Health and Safety Executive (HSE). This framework employs thresholds to classify risk as unacceptable, tolerable, or broadly acceptable and is based on how an individual may perceive their level of risk. The numerical threshold values and a visual adaptation of the framework is seen in Fig. 12. Note that these threshold values have been scaled back from risk per year to risk per 10 min to align with the chosen unit of risk for this research.

REFERENCES

Baker, M. B., and J. G. Dash, 1994: Mechanism of charge transfer between colliding ice particles. *J. Geophys. Res.*, **99**, 10 621–10 626, https://doi.org/10.1029/93JD01633.

Bateman, M. E., and D. M. Mach, 2020: Preliminary detection efficiency and false alarm rate assessment of the Geostationary Lightning Mapper on the *GOES-16* satellite. *J. Appl. Remote Sens.*, **14**, 032406, https://doi.org/10.1117/1.JRS.14.032406.

Biagi, C. J., K. L. Cummins, K. E. Kehoe, and E. P. Krider, 2007: National Lightning Detection Network (NLDN) performance in southern Arizona, Texas, and Oklahoma in 2003–2004. *J. Geophys. Res.*, **112**, D05208, https://doi.org/10.1029/2006JD007341.

Bruning, E. C., and D. R. MacGorman, 2013: Theory and observations of controls on lightning flash size spectra. *J. Atmos. Sci.*, **70**, 4012–4029, https://doi.org/10.1175/JAS-D-12-0289.1.

——, and Coauthors, 2019: Meteorological imagery for the Geostationary Lightning Mapper. *J. Geophys. Res. Atmos.*, **124**, 14 258–14 309, https://doi.org/10.1029/2019JD030874.

Buck, T., A. Nag, and M. J. Murphy, 2014: Improved cloud-to-ground and intracloud lightning detection with the LS7002 Advanced Total lightning sensor. *Proc. WMO Tech. Conf. on Meteorological and Environmental Instruments and Methods of Observation*, Saint Petersburg, Russia, WMO, 8 pp., https://www.wmo.int/pages/prog/www/IMOP/publications/IOM-116_TECO-2014/Session%201/P1_9_Buck_TotalLightningSensor.pdf.

Carey, L. D., M. J. Murphy, T. L. McCormick, and N. W. Demetriades, 2005: Lightning location relative to storm structure in a leading-line trailing stratiform mesoscale convective system. *J. Geophys. Res.*, **110**, D03105, https://doi.org/10.1029/2003JD004371.

Caylor, I. J., and V. Chandrasekar, 1996: Time-varying crystal orientation in thunderstorms observed with multiparameter radar. *IEEE Trans. Geosci. Remote Sens.*, **34**, 847–858, https://doi.org/10.1109/36.508402.

Cummins, K. L., and M. J. Murphy, 2009: An overview of lightning location systems: History, techniques, and data uses with an in-depth look at the U.S. NLDN. *IEEE Trans. Electromagn. Compat.*, **51**, 499–518, https://doi.org/10.1109/TEMC.2009.2023450.

Doviak, R. J., V. Bringi, A. Ryzhkov, A. Zahrai, and D. Zrnić, 2000: Considerations for polarimetric upgrades to operational WSR-88D radars. *J. Atmos. Oceanic Technol.*, **17**, 257–278, https://doi.org/10.1175/1520-0426(2000)017<0257:CFPUTO>2.0.CO;2.

Elsenheimer, C. B., and C. M. Gravelle, 2019: Introducing lightning threat messaging using the *GOES-16* day cloud phase distinction RGB composite. *Wea. Forecasting*, **34**, 1587–1600, https://doi.org/10.1175/WAF-D-19-0049.1.

Emersic, C., and C. P. R. Saunders, 2010: Further laboratory investigations into the relative diffusional growth rate theory of thunderstorm electrification. *Atmos. Res.*, **98**, 327–340, https://doi.org/10.1016/j.atmosres.2010.07.011.

Fleenor, S. A., C. J. Biagi, K. L. Cummins, E. P. Krider, and X. M. Shao, 2009: Characteristics of cloud-to-ground lightning in warm-season thunderstorms in the Central Great Plains. *Atmos. Res.*, **91**, 333–352, https://doi.org/10.1016/j.atmosres.2008.08.011.

Fuelberg, H. E., R. J. Walsh, and A. D. Preston, 2014: The extension of lightning flashes from thunderstorms near Cape Canaveral

Florida. *J. Geophs. Res. Atmos.*, **119**, 9965–9979, https://doi.org/10.1002/2014JD022105.

Giangrande, S. E., T. Toto, A. Bansemer, M. R. Kumjian, S. Mishra, and A. V. Ryzhkov, 2016: Insights into riming and aggregation processes as revealed by aircraft, radar, and disdrometer observations for a 27 April 2011 widespread precipitation event. *J. Geophys. Res. Atmos.*, **121**, 5846–5863, https://doi.org/10.1002/2015JD024537.

Goodman, S. J., and Coauthors, 2013: The GOES-R Geostationary Lightning Mapper (GLM). *Atmos. Res.*, **125–126**, 34–49, https://doi.org/10.1016/j.atmosres.2013.01.006.

Gremillion, M. S., and R. E. Orville, 1999: Thunderstorm characteristics of cloud-to-ground lightning at the Kennedy Space Center, Florida: A study of lightning initiation signatures as indicated by WSR-88D. *Wea. Forecasting*, **14**, 640–649, https://doi.org/10.1175/1520-0434(1999)014<0640:TCOCTG>2.0.CO;2.

Harkema, S., C. J. Schultz, E. B. Berndt, and P. M. Bitzer, 2019: Geostationary Lightning Mapper flash characteristics of electrified snowfall events. *Wea. Forecasting*, **34**, 1571–1585, https://doi.org/10.1175/WAF-D-19-0082.1.

Heinselman, P. L., and A. V. Ryzhkov, 2006: Validation of polarimetric hail detection. *Wea. Forecasting*, **21**, 839–850, https://doi.org/10.1175/WAF956.1.

Hendry, A., and G. C. McCormick, 1976: Radar observations of alignment of precipitation particles by electrostatic fields in thunderstorms. *J. Geophys. Res.*, **81**, 5353–5357, https://doi.org/10.1029/JC081i030p05353.

Holle, R. L., N. W. Demetriades, and A. Nag, 2016: Objective airport warnings over small areas using NLDN cloud and cloud-to-ground lightning data. *Wea. Forecasting*, **31**, 1061–1069, https://doi.org/10.1175/WAF-D-15-0165.1.

Hubbert, J. C., and S. M. Ellis, 2014: Microphysical interpretation of coincident simultaneous and fast alternating horizontal and vertical polarization transmit data. *Eighth European Conf. on Radar in Meteorology and Hydrology (ERAD 2014)*, Garmisch-Partenkirchen, Germany, DWD, http://n2t.net/ark:/85065/d7dn46k1.

——, ——, M. Dixon, and G. Meymaris, 2010: Modeling, error analysis, and evaluation of dual-polarization variables obtained from simultaneous horizontal and vertical polarization transmit radar. Part I: Modeling and antenna errors. *J. Atmos. Oceanic Technol.*, **27**, 1583–1598, https://doi.org/10.1175/2010JTECHA1336.1.

——, ——, W. Chang, S. Rutledge, and M. Dixon, 2014: Modeling and interpretation of S-band ice crystal depolarization signatures from data obtained by simultaneously transmitting horizontally and vertically polarized fields. *J. Appl. Meteor. Climatol.*, **53**, 1659–1677, https://doi.org/10.1175/JAMC-D-13-0158.1.

International Electrotechnical Commission, 2010: Protection against lightning—Part II. Risk management. 2nd ed. IEC, 85 pp.

Kennedy, P. C., and S. A. Rutledge, 2011: S-band dual-polarization radar observations of winter storms. *J. Appl. Meteor. Climatol.*, **50**, 844–858, https://doi.org/10.1175/2010JAMC2558.1.

Koshak, W. J., and R. J. Solakiewicz, 2015: A method for retrieving the ground flash fraction and flash time from satellite lightning mapper observations. *J. Atmos. Oceanic Technol.*, **32**, 79–96, https://doi.org/10.1175/JTECH-D-14-00085.1.

Krehbiel, P. R., T. Chen, S. McCrary, W. Rison, G. Gray, and M. Brook, 1996: The use of dual-channel circular-polarization radar observations for remotely sensing storm electrification. *Meteor. Atmos. Phys.*, **59**, 65–82, https://doi.org/10.1007/BF01032001.

——, J. A. Riousset, V. P. Pasko, R. J. Thomas, W. Rison, M. A. Stanley, and H. E. Edens, 2008: Upward electrical discharges from thunderstorms. *Nat. Geosci.*, **1**, 233–237, https://doi.org/10.1038/ngeo162.

Kuhlman, K. M., D. R. MacGorman, M. I. Biggerstaff, and P. R. Krehbiel, 2009: Lightning initiation in the anvils of two supercell storms. *Geophys. Res. Lett.*, **36**, L07802, https://doi.org/10.1029/2008GL036650.

Kumjian, M. R., 2013: Principles and applications of dual-polarization weather radar. Part III: Artifacts. *J. Oper. Meteor.*, **1**, 265–274, https://doi.org/10.15191/nwajom.2013.0121.

——, and W. Deierling, 2015: Analysis of thundersnow storms over Northern Colorado. *Wea. Forecasting*, **30**, 1469–1490, https://doi.org/10.1175/WAF-D-15-0007.1.

Lang, T. J., and Coauthors, 2017: WMO World record lightning extremes: Longest reported flash distance and longest reported flash duration. *Bull. Amer. Meteor. Soc.*, **98**, 1153–1168, https://doi.org/10.1175/BAMS-D-16-0061.1.

Lengyel, M. M., H. Brooks, R. E. Holle, and M. A. Cooper, 2005: Lightning casualties and their proximity to surrounding cloud-to-ground lightning. *14th Symp. on Education*, Atlanta, GA, Amer. Meteor. Soc., P1.35, https://ams.confex.com/ams/Annual2005/techprogram/paper_85775.htm.

Liu, C., and S. Heckman, 2012: Total lightning data and real-time severe storm prediction. *TECO-2012: WMO Tech. Conf. on Meteorological and Environmental Instruments and Methods of Observation*, Brussels, Belgium, WMO, P5(10), http://www.wmo.int/pages/prog/www/IMOP/publications/IOM-109_TECO-2012/Session5/P5_10_Liu_Total_Lightning_Data_and_Real-Time_Severe_Storm_Prediction.pdf.

Liu, H., and V. Chandrasekar, 2000: Classification of hydrometeors based on polarimetric radar measurements: Development of fuzzy logic and neuro-fuzzy systems, and in situ verification. *J. Atmos. Oceanic Technol.*, **17**, 140–164, https://doi.org/10.1175/1520-0426(2000)017<0140:COHBOP>2.0.CO;2.

Lyons, W. A., E. C. Bruning, T. A. Warner, D. R. MacGorman, S. Edgington, C. Tillier, and J. Mlynarczyk, 2020: Megaflashes: Just how long can a lightning discharge get? *Bull. Amer. Meteor. Soc.*, **101**, E73–E86, https://doi.org/10.1175/BAMS-D-19-0033.1.

MacGorman, D. R., I. R. Apostolakopoulos, N. R. Lund, N. W. S. Demetriades, M. J. Murphy, and P. R. Krehbiel, 2011: The timing of cloud-to-ground lightning relative to total lightning activity. *Mon. Wea. Rev.*, **139**, 3871–3886, https://doi.org/10.1175/MWR-D-11-00047.1.

Mach, D. M., 2019: Geostationary Lightning Mapper Clustering Algorithm Stability. *2019 Geostationary Lightning Mapper Science Team Meeting*, Huntsville, AL, NASA, https://goes-r.nsstc.nasa.gov/home/meeting-agenda-2019.

Medici, G., K. L. Cummins, D. J. Cecil, W. J. Koshak, and S. D. Rudlosky, 2017: The intracloud lightning fraction in the contiguous United States. *Mon. Wea. Rev.*, **145**, 4481–4499, https://doi.org/10.1175/MWR-D-16-0426.1.

Metcalf, J. I., 1997: Temporal and spatial variations of hydrometeor orientation of hydrometeors in thunderstorms. *J. Appl. Meteor.*, **36**, 315–321, https://doi.org/10.1175/1520-0450(1997)036<0315:TASVOH>2.0.CO;2.

Murphy, K. M., 2018: *Assessing Lightning Risk in Outdoor Vulnerable Environments*. Texas Tech University, 143 pp.

——, E. C. Bruning, C. J. Schultz, and J. Vanos, 2021: A spatiotemporal lightning risk assessment using lightning mapping data. *Wea. Climate Soc.*, https://doi.org/10.1175/WCAS-D-20-0021.1, in press.

Nag, A., M. J. Murphy, W. Schulz, and K. L. Cummins, 2015: Lightning locating systems: Insights on characteristics and

validation techniques. *Earth Space Sci.*, **2**, 65–93, https://doi.org/10.1002/2014EA000051.

NOAA, 2020: Advanced Weather Interactive Processing System (AWIPS). Accessed on 16 October 2020, https://vlab.ncep.noaa.gov/web/mdl/awips.

Peterson, M. J., 2019: Research applications for the Geostationary Lightning Mapper operational lightning flash product. *J. Geophys. Res. Atmos.*, **124**, 10 205–10 231, https://doi.org/10.1029/2019JD031054.

——, and Coauthors, 2020: New World Meteorological Organization certified megaflash lightning extremes for flash distance (709 km) and duration (16.73 s) recorded from space. *Geophys. Res. Lett.*, **47**, e2020GL088888, https://doi.org/10.1029/2020GL088888.

Preston, A. D., and H. E. Fuelberg, 2015: Improving lightning cessation guidance using polarimetric radar data. *Wea. Forecasting*, **30**, 308–328, https://doi.org/10.1175/WAF-D-14-00031.1.

Rison, W., R. J. Thomas, P. R. Krehbiel, T. Hamlin, and J. Harlin, 1999: A GPS-based three dimensional lightning mapping system: Initial observations in central New Mexico. *Geophys. Res. Lett.*, **26**, 3573–3576, https://doi.org/10.1029/1999GL010856.

Rudlosky, S. D., S. J. Goodman, K. S. Virts, and E. C. Bruning, 2019: Initial Geostationary Lightning Mapper observations. *Geophys. Res. Lett.*, **46**, 1097–1104, https://doi.org/10.1029/2018GL081052.

Rumpf, C. M., R. S. Longenbaugh, C. E. Henze, J. C. Chavez, and D. L. Mathias, 2019: An algorithmic approach for detecting bolides with the Geostationary Lightning Mapper. *Sensors*, **19**, 1008, https://doi.org/10.3390/s19051008.

Ryzhkov, A. V., 2007: The impact of beam broadening on the quality of radar polarimetric data. *J. Atmos. Oceanic Technol.*, **24**, 729–744, https://doi.org/10.1175/JTECH2003.1.

——, and D. S. Zrnić, 2007: Depolarization in ice crystals and its effect on radar polarimetric measurements. *J. Atmos. Oceanic Technol.*, **24**, 1256–1267, https://doi.org/10.1175/JTECH2034.1.

Sanderson, D. L., E. D. White, A. J. Geyer, W. P. Roeder, and A. J. Gutman, 2020: Optimizing the lightning warning radii at spaceport Florida. *Wea. Forecasting*, **35**, 523–536, https://doi.org/10.1175/WAF-D-19-0129.1.

Saunders, C. P. R., H. Bax-Norman, C. Emersic, E. E. Avila, and N. E. Castellano, 2006: Laboratory studies of the effect of cloud conditions on graupel/crystal charge transfer in thunderstorm electrification. *Quart. J. Roy. Meteor. Soc.*, **132**, 2653–2673, https://doi.org/10.1256/qj.05.218.

Schultz, C. J., and B. C. Carcione, 2020: Rumble heard 'Round the Valley. Wide Word of SPoRT blog post. Accessed 20 April 2020, https://nasasport.wordpress.com/2020/04/20/the-rumble-heard-round-the-valley/.

——, G. T. Stano, P. J. Meyer, B. C. Carcione, and T. Barron, 2017: Lightning decision support using VHF total lightning mapping and NLDN cloud-to-ground data in North Alabama. *J. Oper. Meteor.*, **5**, 134–145, https://doi.org/10.15191/nwajom.2017.0511.

Scott, R. D., P. R. Krehbiel, and W. Rison, 2001: The use of simultaneous horizontal and vertical transmissions for dual-polarization radar meteorological observations. *J. Atmos. Oceanic Technol.*, **18**, 629–648, https://doi.org/10.1175/1520-0426(2001)018<0629:TUOSHA>2.0.CO;2.

Stano, G. T., H. E. Fuelberg, and W. P. Roeder, 2010: Developing empirical lightning cessation forecast guidance for the Cape Canaveral Air Force Station and Kennedy Space Center. *J. Geophys. Res.*, **115**, D09205, https://doi.org/10.1029/2009JD013034.

——, M. R. Smith, and C. J. Schultz, 2019: Development and evaluation of the GLM stoplight product for lightning safety. *J. Oper. Meteor.*, **7**, 92–104, https://doi.org/10.15191/nwajom.2019.0707.

Steiger, S. M., R. E. Orville, and L. D. Carey, 2007: Total lightning signatures of thunderstorm intensity over North Texas. Part II: Mesoscale convective systems. *Mon. Wea. Rev.*, **135**, 3303–3324, https://doi.org/10.1175/MWR3483.1.

Straka J. M., D. S. Zrnić, and A. V. Ryzhkov, 2000: Bulk hydrometeor classification and quantification using polarimetric radar data: Synthesis of relations. *J. Appl. Meteor.*, **39**, 1341–1372, https://doi.org/10.1175/1520-0450(2000)039<1341:BHCAQU>2.0.CO;2.

Takahashi, T., 1978: Riming electrification as a charge generation mechanism in thunderstorms. *J. Atmos. Sci.*, **35**, 1536–1548, https://doi.org/10.1175/1520-0469(1978)035<1536:REAACG>2.0.CO;2.

Thompson, E. J., S. A. Rutledge, B. Dolan, V. Chandrasekar, and B. L. Cheong, 2014: A dual-polarization radar hydrometeor classification algorithm for winter precipitation. *J. Atmos. Oceanic Technol.*, **31**, 1457–1481, https://doi.org/10.1175/JTECH-D-13-00119.1.

Unidata, 2020: Integrated Data Viewer. Accessed 3 June 2020, https://doi.org/10.5065/D6H70CW6.

Vincent, B. R., L. D. Carey, D. Schneider, K. Keeter, and R. Gonski, 2003: Using WSR-88D reflectivity data for the prediction of cloud-to-ground lightning: A North Carolina study. *Natl. Wea. Dig.*, **27**, 35–44.

Vivekanandan, J., D. S. Zrnić, S. M. Ellis, R. Oye, A. V. Ryzhkov, and J. Straka, 1999: Cloud microphysics retrieval using S-band dual-polarization radar measurements. *Bull. Amer. Meteor. Soc.*, **80**, 381–388, https://doi.org/10.1175/1520-0477(1999)080<0381:CMRUSB>2.0.CO;2.

Weiss, S. A., D. R. MacGorman, and K. M. Calhoun, 2012: Lightning in the anvils of supercell thunderstorms. *Mon. Wea. Rev.*, **140**, 2064–2079, https://doi.org/10.1175/MWR-D-11-00312.1.

Woodard, C. J., L. D. Carey, W. A. Petersen, and W. P. Roeder, 2012: Operational utility of dual-polarization variables in lightning initiation forecasting. *Electron. J. Oper. Meteor.*, **13**, 79–102.

Zrnić, D. S., N. Balakrishnan, C. L. Ziegler, V. N. Bringi, K. Aydin, and T. Matejka, 1993: Polarimetric signatures in the stratiform region of a mesoscale convective system. *J. Appl. Meteor.*, **32**, 678–693, https://doi.org/10.1175/1520-0450(1993)032<0678:PSITSR>2.0.CO;2.